Annals of Nuclear Energy 64 (2014) 230–243

Contents lists available at ScienceDirect

Annals of Nuclear Energy

journal homepage: www.elsevier.com/locate/anucene

Technical Note

NEMSQR: A 3-D multi group diffusion theory code based on nodal expansion method for square geometry

Tej Singh *, Tanay Mazumdar, Paritosh Pandey

Reactor Group, Bhabha Atomic Research Centre, Mumbai 400085, India

ARTICLE INFO

Article history:
Received 3 June 2013
Received in revised form 18 September 2013
Accepted 25 September 2013
Available online 6 November 2013

Keywords:
Lattice
Assembly
Node
Mesh
Homogenization

ABSTRACT

A three dimensional, multigroup, neutron diffusion theory based computer code NEMSQR (Nodal Expansion Method for SQuare geometry) is developed for square geometry in order to perform reactor core calculation. The code is based on Nodal Expansion Method (NEM). In this method, an inhomogeneous matrix equation, which involves spatial moments of nodal flux distribution and surface averaged partial currents across the nodal surfaces, is derived using fourth order polynomial approximation to spatial dependence of nodal flux. Discontinuity factor is incorporated into the code to reduce homogenization error. This code is used for calculation of effective multiplication factor, neutron flux (both direct and adjoint flux), integral kinetics parameters and subcritical count in presence of external neutron source. The numerical studies reported here for several benchmark problems related to light water reactor as well as fast breeder reactor demonstrate the accuracy of the code.

1. Introduction

Neutron flux or power distribution inside reactor core during steady as well as transient state is calculated solving few energy group, steady state or time dependent neutron diffusion equation respectively. Since reactor consists of lots of heterogeneities in a sense that there are varieties of materials used as fuel, clad, coolant, moderator, reflector and other structural components in core, the calculation is not at all straightforward. In first step of calculation, reactor is divided into a number of regions, normally equal to the size of an assembly, and then materials of fuel, clad, coolant etc. in the respective regions are replaced with an equivalent material whose homogenized cross sections are generated using a neutron transport theory based lattice code. Finally, three dimensional, multigroup diffusion equation is solved using the generated homogenized cross sections. Several numerical methods such as finite difference method (FDM) (Menon et al., 1981), finite element method (FEM) (Jagannathan, 1983) and nodal method have been developed to solve the diffusion equation. FDM is quite a straightforward method to solve the diffusion equation though it invariably requires the mesh size to be equal to diffusion length of the material. Hence, large number of mesh is required in case of light water reactors and subsequently computational time becomes quite long. Nodal method is a suitable alternative in this regard. In this method, the diffusion equation is integrated over large homogenized region known as 'nodes' to obtain a nodal balance equation with average surface currents and fluxes as unknowns. In the conventional nodal methods (Delp et al., 1964, Goldstein et al., 1967), the currents are eliminated from the balance equation using spatial coupling coefficients, which are defined as the ratio of average surface currents and fluxes in a node. The spatial coupling coefficients are estimated a priori by applying certain assumptions or by using auxiliary fine mesh calculations. This makes the method less accurate, still they provide acceptable results for static problems. But then conventional nodal methods are certainly not suitable for kinetics calculations, as the coupling coefficients are likely to change from time to time, and thus are to be calculated repeatedly. In order to circumvent the problem of recalculation of coupling coefficients, many higher order nodal methods such as Nodal Expansion Method (NEM) (Finnemann, 1975, 1977), polynomial method (Sims and Henry, 1976, Shober and Henry, 1976), analytical nodal method (ANM) (Shober et al., 1977), Green's function method (Lawrence, 1979) have been developed. ANM is based on analytical solution of transverse integrated diffusion equation for each node. However, this method, due to its complexity, is restricted to not more than two energy groups. NEM is an example of first generation polynomial nodal method. One of its main advantages is that there is no restriction on number of energy groups. Accuracy of both ANM and NEM are comparable. In these modern nodal methods, three dimensional diffusion equation is converted into a set of three one dimensional equations by integrating the diffusion equation over two directions transverse to each coordinate axis and the set of one dimensional equations thus

* Corresponding author. Tel.: +91 22 25594196; fax: +91 22 25505311.
E-mail address: tejsingh.956@gmail.com (T. Singh).

0306-4549/$ - see front matter © 2013 Elsevier Ltd. All rights reserved.
http://dx.doi.org/10.1016/j.anucene.2013.09.041

obtained is then solved. Currents, in these methods, are treated explicitly to obtain couplings between adjacent nodes. These methods are computationally efficient as the calculation of current is simple and inexpensive. The iterative matrix is also very simple unlike the one obtained in FDM. Since size of nodes is equal to the size of assemblies in reactor, computation time is also reduced by a factor of two. Moreover, the power distributions obtained from these methods are very accurate. This paper is written in following way. In Section 2, Nodal Expansion Method (NEM) proposed by Lawrence, 1986 is briefly described. The next section is dedicated to the calculation of transverse leakage moment. Subsequent sections describe the importance and incorporation of discontinuity factor in the code NEMSQR, how the code calculates effective multiplication factor, neutron flux (both direct and adjoint flux), fission power distribution, integral kinetics parameters and subcritical count in presence of external neutron source. The code is written for static problem and is benchmarked against various such problems available in literature. A good agreement is observed between results of the code and benchmark problems, discussed in Section 8.

2. Nodal expansion method

In this method, reactor is divided into k number of homogeneous, rectangular nodes. Cross sections within the nodes are assumed to be constant. Let us consider a node k as shown in Fig. 1. For kth node, multigroup steady state neutron diffusion equation can be written as

$$\vec{\nabla}\vec{J}_g^k(x,y,z)+\sum_{rg}^{k}\phi_g^k(x,y,z)=Q_g^k(x,y,z)$$
$$\Rightarrow \frac{\partial}{\partial x}\left(J_{gx}^k(x,y,z)\right)+\frac{\partial}{\partial y}\left(J_{gy}^k(x,y,z)\right)+\frac{\partial}{\partial z}\left(J_{gz}^k(x,y,z)\right)+\sum_{rg}^{k}\phi_g^k(x,y,z)=Q_g^k(x,y,z) \quad (1)$$

where total source, $Q_g^k(x,y,z)=\frac{\chi_g}{\lambda}\sum_{g'=1}^{G}\nu\sum_{fg'}^{k}\phi_{g'}^k(x,y,z)+\sum_{\substack{g'=1\\g'\neq g}}^{G}\sum_{sg'\to g}^{k}\phi_{g'}^k(x,y,z)$. In order to make Eq. (1) one dimensional (let's take x direction), it is integrated over two transverse directions i.e. y and z directions and after dividing by $\Delta y_k\Delta z_k$, following equation is obtained.

$$\frac{d}{dx}J_{gx}^k(x)+\frac{1}{\Delta y_k}L_{gy}^k(x)+\frac{1}{\Delta z_k}L_{gz}^k(x)+\sum_{rg}^{k}\phi_{gx}^k(x)=Q_{gx}^k(x) \quad (2)$$

where

$$\left.\begin{aligned}
J_{gx}^k(x)&=\frac{1}{\Delta y_k\Delta z_k}\int_{-\frac{\Delta y_k}{2}}^{\frac{\Delta y_k}{2}}\int_{-\frac{\Delta z_k}{2}}^{\frac{\Delta z_k}{2}}J_{gx}^k(x,y,z)dy\,dz,\\
L_{gy}^k(x)&=\frac{1}{\Delta z_k}\int_{-\frac{\Delta z_k}{2}}^{\frac{\Delta z_k}{2}}\left(J_{gy}^k\left(x,\tfrac{\Delta y_k}{2},z\right)-J_{gy}^k\left(x,-\tfrac{\Delta y_k}{2},z\right)\right)dz,\\
L_{gz}^k(x)&=\frac{1}{\Delta y_k}\int_{-\frac{\Delta y_k}{2}}^{\frac{\Delta y_k}{2}}\left(J_{gz}^k\left(x,y,\tfrac{\Delta z_k}{2}\right)-J_{gz}^k\left(x,y,-\tfrac{\Delta z_k}{2}\right)\right)dy,\\
\phi_{gx}^k(x)&=\frac{1}{\Delta y_k\Delta z_k}\int_{-\frac{\Delta y_k}{2}}^{\frac{\Delta y_k}{2}}\int_{-\frac{\Delta z_k}{2}}^{\frac{\Delta z_k}{2}}\phi_g^k(x,y,z)dy\,dz,\\
Q_{gx}^k(x)&=\frac{1}{\Delta y_k\Delta z_k}\int_{-\frac{\Delta y_k}{2}}^{\frac{\Delta y_k}{2}}\int_{-\frac{\Delta z_k}{2}}^{\frac{\Delta z_k}{2}}Q_g^k(x,y,z)dy\,dz
\end{aligned}\right\} \quad (2.1)$$

Now, gth group neutron flux in kth node, $\phi_{gx}^k(x)$ is expanded in terms of polynomials up to fourth order as following.

$$\phi_{gx}^k(x)\approx\overline{\phi_g^k}f_0(x)+\sum_{i=1}^{4}a_{gxi}^k f_i(x) \quad (3)$$

where node averaged flux, $\overline{\phi_g^k}=\frac{1}{\Delta x_k\Delta y_k\Delta z_k}\int_{-\frac{\Delta x_k}{2}}^{\frac{\Delta x_k}{2}}\int_{-\frac{\Delta y_k}{2}}^{\frac{\Delta y_k}{2}}\int_{-\frac{\Delta z_k}{2}}^{\frac{\Delta z_k}{2}}\phi_g^k(x,y,z)\,dx\,dy\,dz$ and the polynomials are $f_0(x)=1$, $f_1(x)=\frac{x}{\Delta x_k}=\xi$, $f_2(x)=3\xi^2-\frac{1}{4}$, $f_3(x)=\xi\left(\xi^2-\frac{1}{4}\right)$ and $f_4(x)=\left(\xi^2-\frac{1}{20}\right)\left(\xi^2-\frac{1}{4}\right)$. These polynomials are chosen in such a way that the volume average of $\phi_g^k(x,y,z)$ yields exactly $\overline{\phi_g^k}$ which implies

$$\left.\begin{aligned}\frac{1}{\Delta x_k}\int_{-\frac{\Delta x_k}{2}}^{\frac{\Delta x_k}{2}}f_n(x)dx=1 \quad &\text{for} \quad n=0\\ =0 \quad &\text{for} \quad n>0\end{aligned}\right\} \quad (4)$$

Flux expansion coefficients, a_{gxi}^k are to be found out from boundary conditions. Let us define $\phi_{gx}^k(x=\pm\frac{\Delta x_k}{2})=\phi_{gx\pm}^k$. Therefore,

$$\phi_{gx}^k\left(x=+\frac{\Delta x_k}{2}\right)=\phi_{gx+}^k=\overline{\phi_g^k}+a_{gx1}^k f_1\left(\frac{\Delta x_k}{2}\right)+a_{gx2}^k f_2\left(\frac{\Delta x_k}{2}\right)+a_{gx3}^k f_3\left(\frac{\Delta x_k}{2}\right)+a_{gx4}^k f_4\left(\frac{\Delta x_k}{2}\right)$$
$$\Rightarrow\ a_{gx1}^k+a_{gx2}^k=2\phi_{gx+}^k-2\overline{\phi_g^k} \quad (5)$$

and

$$\phi_{gx}^k\left(x=-\frac{\Delta x_k}{2}\right)=\phi_{gx-}^k=\overline{\phi_g^k}+a_{gx1}^k f_1\left(-\frac{\Delta x_k}{2}\right)+a_{gx2}^k f_2\left(-\frac{\Delta x_k}{2}\right)+a_{gx3}^k f_3\left(-\frac{\Delta x_k}{2}\right)+a_{gx4}^k f_4\left(-\frac{\Delta x_k}{2}\right)$$
$$\Rightarrow\ a_{gx1}^k-a_{gx2}^k=2\overline{\phi_g^k}-2\phi_{gx-}^k \quad (6)$$

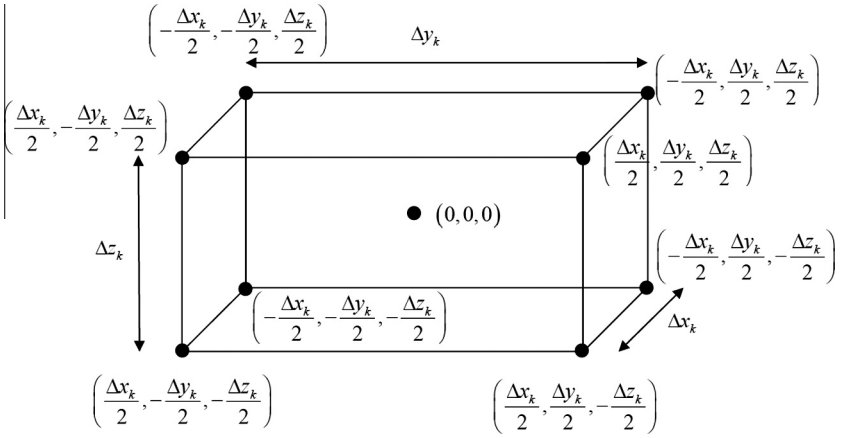

Fig. 1. (0,0,0) Centred kth node of dimension $\Delta x_k\times\Delta y_k\times\Delta z_k$, considered in nodal expansion method.

Solving Eqs. (5) and (6),

$$\left.\begin{aligned} a^k_{gx1} &= \phi^k_{gx+} - \phi^k_{gx-} \\ a^k_{gx2} &= \phi^k_{gx+} + \phi^k_{gx-} - 2\overline{\phi^k_g} \end{aligned}\right\} \tag{7}$$

Higher order coefficients a^k_{gx3} and a^k_{gx4} are determined by applying a weighted residual method in following manner. Multiplying Eq. (2) with a weight $w_i(x)$ and then taking x average on both sides,

$$\left\langle w_i(x)\frac{d}{dx}\overline{J^k_{gx}}(x)\right\rangle + \frac{1}{\Delta y_k}L^k_{gyxi} + \frac{1}{\Delta z_k}L^k_{gzxi} + \sum_{rg}^{k}\overline{\phi^k_{gxi}} = \overline{Q^k_{gxi}} \tag{8}$$

$$\left.\begin{aligned} &\text{where } \left\langle w_i(x)\tfrac{d}{dx}J^k_{gx}(x)\right\rangle = \tfrac{1}{\Delta x_k}\int_{-\frac{\Delta x_k}{2}}^{\frac{\Delta x_k}{2}} w_i(x)\tfrac{d}{dx}J^k_{gx}(x)dx, \\ &L^k_{gyxi} = \tfrac{1}{\Delta x_k}\int_{-\frac{\Delta x_k}{2}}^{\frac{\Delta x_k}{2}} w_i(x)L^k_{gy}(x)dx, \\ &L^k_{gzxi} = \tfrac{1}{\Delta x_k}\int_{-\frac{\Delta x_k}{2}}^{\frac{\Delta x_k}{2}} w_i(x)L^k_{gz}(x)dx, \\ &\overline{\phi^k_{gxi}} = \tfrac{1}{\Delta x_k}\int_{-\frac{\Delta x_k}{2}}^{\frac{\Delta x_k}{2}} w_i(x)\phi^k_{gx}(x)dx, \\ &\overline{Q^k_{gxi}} = \tfrac{1}{\Delta x_k}\int_{-\frac{\Delta x_k}{2}}^{\frac{\Delta x_k}{2}} w_i(x)Q^k_{gx}(x)dx \end{aligned}\right\} \tag{8.1}$$

For $i=1,\ w_i(x)=w_1(x)=f_1(x)=\frac{x}{\Delta x_k}$, integrating 1st term of Eq. (8) by integration by parts and rewriting the equation,

$$\frac{1}{2\Delta x_k}T^k_{gx} + \frac{D^k_g}{\Delta x_k}\frac{a^k_{gx1}}{\Delta x_k} + \frac{1}{\Delta y_k}L^k_{gyx1} + \frac{1}{\Delta z_k}L^k_{gzx1} + \sum_{rg}^{k}\overline{\phi^k_{gx1}} = \overline{Q^k_{gx1}}$$

$$\Rightarrow \frac{1}{2\Delta x_k}T^k_{gx} + \frac{D^k_g}{\Delta x_k}\frac{a^k_{gx1}}{\Delta x_k} + L^k_{gx1} + \sum_{rg}^{k}\overline{\phi^k_{gx1}} = \overline{Q^k_{gx1}} \tag{9}$$

where $T^k_{gx} = \left(J^k_{gx+} + J^k_{gx-}\right)$ and $L^k_{gx1} = \frac{1}{\Delta y_k}L^k_{gyx1} + \frac{1}{\Delta z_k}L^k_{gzx1}$. Now substituting $\phi^k_{gx}(x)$ in $\overline{\phi^k_{gx1}}$ with Eq. (3) and then integrating,

$$\overline{\phi^k_{gx1}} = a^k_{gx1}\frac{1}{12} - a^k_{gx3}\frac{1}{120} \Rightarrow a^k_{gx3} = 10a^k_{gx1} - 120\overline{\phi^k_{gx1}} \Rightarrow a^k_{gx3}$$
$$= 10\phi^k_{gx+} - 10\phi^k_{gx-} - 120\overline{\phi^k_{gx1}} \quad \text{(using Eq. (7))} \tag{10}$$

For $i=2,\ w_i(x)=w_2(x)=f_2(x)=3\left(\frac{x}{\Delta x_k}\right)^2-\frac{1}{4}$, following equations, analogue of Eqs. (9) and (10), are obtained.

$$\frac{1}{2\Delta x_k}L^k_{gx} + \frac{3D^k_g}{\Delta x^2_k}a^k_{gx2} + L^k_{gx2} + \sum_{rg}^{k}\overline{\phi^k_{gx2}} = \overline{Q^k_{gx2}} \tag{11}$$

where $L^k_{gx} = \left(J^k_{gx+} - J^k_{gx-}\right)$ and $L^k_{gx2} = \frac{1}{\Delta y_k}L^k_{gyx2} + \frac{1}{\Delta z_k}L^k_{gzx2}$. and

$$\overline{\phi^k_{gx2}} = a^k_{gx2}\frac{1}{20} - a^k_{gx4}\frac{1}{700} \Rightarrow a^k_{gx4} = 35a^k_{gx2} - 700\overline{\phi^k_{gx2}} \Rightarrow a^k_{gx4}$$
$$= 35\phi^k_{gx+} + 35\phi^k_{gx-} - 70\overline{\phi^k_g} - 700\overline{\phi^k_{gx2}} \quad \text{(using Eq. (7))} \tag{12}$$

Integrating Eq. (2) over x and writing net current in $\pm x$ direction ($J^k_{gx\pm}$) as the difference between outgoing ($J^k_{gx\pm,out}$) and incoming ($J^k_{gx\pm,in}$) partial currents i.e. $J^k_{gx\pm,out} - J^k_{gx\pm,in} = \pm J^k_{gx\pm} = \pm\frac{1}{\Delta y_k\Delta z_k}\int_{-\frac{\Delta y_k}{2}}^{\frac{\Delta y_k}{2}}\int_{-\frac{\Delta z_k}{2}}^{\frac{\Delta z_k}{2}} J^k_{gx}\left(\pm\frac{\Delta x_k}{2}, y, z\right)dy\,dz$, (similar for net currents in y and z directions)

$$\overline{\phi^k_g} = \frac{\overline{Q^k_g}}{\sum^k_{rg}} + \begin{pmatrix} -\frac{1}{\sum^k_{rg}\Delta x_k}J^k_{gx+,out} + \frac{1}{\sum^k_{rg}\Delta x_k}J^k_{gx+,in} + \frac{1}{\sum^k_{rg}\Delta x_k}J^k_{gx-,in} - \frac{1}{\sum^k_{rg}\Delta x_k}J^k_{gx-,out} \\ -\frac{1}{\sum^k_{rg}\Delta y_k}J^k_{gy+,out} + \frac{1}{\sum^k_{rg}\Delta y_k}J^k_{gy+,in} + \frac{1}{\sum^k_{rg}\Delta y_k}J^k_{gy-,in} - \frac{1}{\sum^k_{rg}\Delta y_k}J^k_{gy-,out} \\ -\frac{1}{\sum^k_{rg}\Delta z_k}J^k_{gz+,out} + \frac{1}{\sum^k_{rg}\Delta z_k}J^k_{gz+,in} + \frac{1}{\sum^k_{rg}\Delta z_k}J^k_{gz-,in} - \frac{1}{\sum^k_{rg}\Delta z_k}J^k_{gz-,out} \end{pmatrix} \tag{13.1}$$

$$\text{where } \overline{Q^k_g} = \frac{\chi_g}{\lambda}\sum_{g'=1}^{G}\nu\sum_{fg'}^{k}\overline{\phi^k_{g'}} + \sum_{\substack{g'=1\\ g'\neq g}}^{G}\sum_{sg'\to g}^{k}\overline{\phi^k_{g'}} \tag{13.2}$$

Using $J^k_{gx\pm,out} - J^k_{gx\pm,in} = \pm J^k_{gx\pm}$, $\overline{\phi^k_{gx1}}$ is derived from Eq. (9)

$$\begin{aligned} \overline{\phi^k_{gx1}} = {} & \frac{\overline{Q^k_{gx1}} - L^k_{gx1}}{\sum_{rg}^{k}} - \frac{1}{\sum_{rg}^{k}}\left(\frac{1}{2\Delta x_k} + \frac{2D^k_g}{\Delta x^2_k}\right)J^k_{gx+,out} \\ & + \frac{1}{\sum_{rg}^{k}}\left(\frac{1}{2\Delta x_k} + \frac{2D^k_g}{\Delta x^2_k}\right)J^k_{gx-,out} + \frac{1}{\sum_{rg}^{k}}\left(\frac{1}{2\Delta x_k} - \frac{2D^k_g}{\Delta x^2_k}\right)J^k_{gx+,in} \\ & - \frac{1}{\sum_{rg}^{k}}\left(\frac{1}{2\Delta x_k} - \frac{2D^k_g}{\Delta x^2_k}\right)J^k_{gx-,in} \end{aligned} \tag{14.1}$$

$$\text{where } \overline{Q^k_{gx1}} = \frac{\chi_g}{\lambda}\sum_{g'=1}^{G}\nu\sum_{fg'}^{k}\overline{\phi^k_{g'x1}} + \sum_{\substack{g'=1\\ g'\neq g}}^{G}\sum_{sg'\to g}^{k}\overline{\phi^k_{g'x1}} \tag{14.2}$$

and $\overline{\phi^k_{gx2}}$ is derived from Eq. (11).

$$\begin{aligned} \overline{\phi^k_{gx2}} = {} & \frac{\overline{Q^k_{gx2}} - L^k_{gx2}}{\sum_{rg}^{k}} + \frac{6D^k_g}{\left(\sum_{rg}^{k}\Delta x_k\right)^2}\overline{Q^k_g} \\ & - \frac{1}{\sum_{rg}^{k}}\left(\frac{1}{2\Delta x_k} + \frac{6D^k_g}{\Delta x^2_k} + \frac{6D^k_g}{\sum_{rg}^{k}\Delta x^3_k}\right)J^k_{gx+,out} \\ & - \frac{1}{\sum_{rg}^{k}}\left(\frac{1}{2\Delta x_k} + \frac{6D^k_g}{\Delta x^2_k} + \frac{6D^k_g}{\sum_{rg}^{k}\Delta x^3_k}\right)J^k_{gx-,out} \\ & - \frac{6D^k_g}{\left(\sum_{rg}^{k}\Delta x_k\right)^2\Delta y_k}J^k_{gy+,out} - \frac{6D^k_g}{\left(\sum_{rg}^{k}\Delta x_k\right)^2\Delta y_k}J^k_{gy-,out} \\ & - \frac{6D^k_g}{\left(\sum_{rg}^{k}\Delta x_k\right)^2\Delta z_k}J^k_{gz+,out} - \frac{6D^k_g}{\left(\sum_{rg}^{k}\Delta x_k\right)^2\Delta z_k}J^k_{gz-,out} \\ & + \frac{1}{\sum_{rg}^{k}}\left(\frac{1}{2\Delta x_k} - \frac{6D^k_g}{\Delta x^2_k} + \frac{6D^k_g}{\sum_{rg}^{k}\Delta x^3_k}\right)J^k_{gx+,in} \\ & + \frac{1}{\sum_{rg}^{k}}\left(\frac{1}{2\Delta x_k} - \frac{6D^k_g}{\Delta x^2_k} + \frac{6D^k_g}{\sum_{rg}^{k}\Delta x^3_k}\right)J^k_{gx-,in} \\ & + \frac{6D^k_g}{\left(\sum_{rg}^{k}\Delta x_k\right)^2\Delta y_k}J^k_{gy+,in} + \frac{6D^k_g}{\left(\sum_{rg}^{k}\Delta x_k\right)^2\Delta y_k}J^k_{gy-,in} \\ & + \frac{6D^k_g}{\left(\sum_{rg}^{k}\Delta x_k\right)^2\Delta z_k}J^k_{gz+,in} + \frac{6D^k_g}{\left(\sum_{rg}^{k}\Delta x_k\right)^2\Delta z_k}J^k_{gz-,in} \end{aligned} \tag{15.1}$$

$$\text{where } \overline{Q^k_{gx2}} = \frac{\chi_g}{\lambda}\sum_{g'=1}^{G}\nu\sum_{fg'}^{k}\overline{\phi^k_{g'x2}} + \sum_{\substack{g'=1\\ g'\neq g}}^{G}\sum_{sg'\to g}^{k}\overline{\phi^k_{g'x2}} \tag{15.2}$$

Outgoing partial currents through both x-directed surfaces of kth node in terms of flux expansion coefficients are

$$\left.\begin{aligned} J^k_{gx+,out} &= -D^k_g\left(\frac{d}{dx}\phi^k_{gx}(x)\right)_{x=\frac{\Delta x_k}{2}} + J^k_{gx+,in} \\ &\approx -\frac{D^k_g}{\Delta x_k}\left(a^k_{gx1} + 3a^k_{gx2} + \frac{1}{2}a^k_{gx3} + \frac{1}{5}a^k_{gx4}\right) + J^k_{gx+,in} \\ J^k_{gx-,out} &= +D^k_g\left(\frac{d}{dx}\phi^k_{gx}(x)\right)_{x=-\frac{\Delta x_k}{2}} + J^k_{gx-,in} \\ &\approx \frac{D^k_g}{\Delta x_k}\left(a^k_{gx1} - 3a^k_{gx2} + \frac{1}{2}a^k_{gx3} - \frac{1}{5}a^k_{gx4}\right) + J^k_{gx-,in} \end{aligned}\right\} \tag{16}$$

Using Eqs. (7), (10) and (12) for expansion coefficients along with Eqs. (13.1), (14.1) and (15.1) for node averaged flux and its moments, both outgoing x-directed partial currents can be expressed in terms of incoming partial currents, source and its moments and leakage moments. Similar expressions can be obtained for y- and z-directed outgoing partial current pairs. All these equations are clubbed together to form a single matrix equation as following.

$$\begin{pmatrix} a_{11} & a_{12} & a_{13} & a_{14} & a_{15} & a_{16} \\ a_{21} & a_{22} & a_{23} & a_{24} & a_{25} & a_{26} \\ a_{31} & a_{32} & a_{33} & a_{34} & a_{35} & a_{36} \\ a_{41} & a_{42} & a_{43} & a_{44} & a_{45} & a_{46} \\ a_{51} & a_{52} & a_{53} & a_{54} & a_{55} & a_{56} \\ a_{61} & a_{62} & a_{63} & a_{64} & a_{65} & a_{66} \end{pmatrix} \begin{pmatrix} J^k_{gx+,out} \\ J^k_{gx-,out} \\ J^k_{gy+,out} \\ J^k_{gy-,out} \\ J^k_{gz+,out} \\ J^k_{gz-,out} \end{pmatrix}$$

$$= \begin{pmatrix} b_{11} & b_{12} & b_{13} & b_{14} & b_{15} & b_{16} & b_{17} \\ b_{21} & b_{22} & b_{23} & b_{24} & b_{25} & b_{26} & b_{27} \\ b_{31} & b_{32} & b_{33} & b_{34} & b_{35} & b_{36} & b_{37} \\ b_{41} & b_{42} & b_{43} & b_{44} & b_{45} & b_{46} & b_{47} \\ b_{51} & b_{52} & b_{53} & b_{54} & b_{55} & b_{56} & b_{57} \\ b_{61} & b_{62} & b_{63} & b_{64} & b_{65} & b_{66} & b_{67} \end{pmatrix} \begin{pmatrix} \overline{Q^k_g} \\ \overline{Q^k_{gx1}} - L^k_{gx1} \\ \overline{Q^k_{gx2}} - L^k_{gx2} \\ \overline{Q^k_{gy1}} - L^k_{gy1} \\ \overline{Q^k_{gy2}} - L^k_{gy2} \\ \overline{Q^k_{gz1}} - L^k_{gz1} \\ \overline{Q^k_{gz2}} - L^k_{gz2} \end{pmatrix}$$

$$+ \begin{pmatrix} c_{11} & c_{12} & c_{13} & c_{14} & c_{15} & c_{16} \\ c_{21} & c_{22} & c_{23} & c_{24} & c_{25} & c_{26} \\ c_{31} & c_{32} & c_{33} & c_{34} & c_{35} & c_{36} \\ c_{41} & c_{42} & c_{43} & c_{44} & c_{45} & c_{46} \\ c_{51} & c_{52} & c_{53} & c_{54} & c_{55} & c_{56} \\ c_{61} & c_{62} & c_{63} & c_{64} & c_{65} & c_{66} \end{pmatrix} \begin{pmatrix} J^k_{gx+,in} \\ J^k_{gx-,in} \\ J^k_{gy+,in} \\ J^k_{gy-,in} \\ J^k_{gz+,in} \\ J^k_{gz-,in} \end{pmatrix}$$

$$\Rightarrow [A]_{6\times6}\left[J^k_{g,out}\right]_{6\times1} = [B]_{6\times7}\left[Q^k_g - L^k_g\right]_{7\times1} + [C]_{6\times6}\left[J^k_{g,in}\right]_{6\times1}$$

$$\Rightarrow \left[J^k_{g,out}\right]_{6\times1} = \left[A^k_g\right]^{-1}_{6\times6}\left[B^k_g\right]_{6\times7}\left[Q^k_g - L^k_g\right]_{7\times1} + \left[A^k_g\right]^{-1}_{6\times6}\left[C^k_g\right]_{6\times6}\left[J^k_{g,in}\right]_{6\times1}$$

$$\Rightarrow \left[J^k_{g,out}\right]_{6\times1} = \left[P^k_g\right]_{6\times7}\left[Q^k_g - L^k_g\right]_{7\times1} + \left[R^k_g\right]_{6\times6}\left[J^k_{g,in}\right]_{6\times1} \quad (17)$$

Matrix elements (a_{ij}, b_{ij}, c_{ij}) are given in Appendix A. These elements are computed and stored for nodes characterized by its dimensions along x, y, z directions and homogenized material present in the node.

3. Calculation of transverse leakage moments

Leakage moment terms of the matrix $\left[Q^k_g - L^k_g\right]_{7\times1}$ in Eq. (17) i.e. L^k_{gx1}, L^k_{gx2}, L^k_{gy1}, L^k_{gy2}, L^k_{gz1} and L^k_{gz2} are derived in this section. Like $\phi^k_{gx}(x)$ in Eq. (3), y-directed leakage $L^k_{gy}(x)$ is also expanded in terms of polynomials, but here it is restricted up to second order as the accuracy achieved in calculation is insignificant with respect to computational effort involved in higher order expansion.

$$L^k_{gy}(x) = \overline{L^k_{gy}} f_0(x) + \sum_{i=1}^{2} b^k_{gyi} f_i(x)$$

$$= \overline{L^k_{gy}} + b^k_{gy1}\left(\frac{x}{\Delta x_k}\right) + b^k_{gy2}\left(3\left(\frac{x}{\Delta x_k}\right)^2 - \frac{1}{4}\right) \quad (18)$$

The leakage expansion coefficients b^k_{gy1} and b^k_{gy2} are determined by calculating average y-directed leakage of $(k-1)$th and $(k+1)$th node as following.

$$\overline{L^{k-1}_{gy}} = \frac{\int_{-\left(\frac{\Delta x_k}{2}+\Delta x_{k-1}\right)}^{-\frac{\Delta x_k}{2}} L^k_{gy}(x)\,dx}{\int_{-\left(\frac{\Delta x_k}{2}+\Delta x_{k-1}\right)}^{-\frac{\Delta x_k}{2}} dx} = \frac{1}{\Delta x_{k-1}} \int_{-\left(\frac{\Delta x_k}{2}+\Delta x_{k-1}\right)}^{-\frac{\Delta x_k}{2}} L^k_{gy}(x)\,dx$$

$$\Rightarrow \overline{L^{k-1}_{gy}} = \overline{L^k_{gy}} - \frac{b^k_{gy1}}{2}\alpha_{1x} + 3b^k_{gy2}\beta_{1x} \quad (19)$$

where $\alpha_{1x} = \left(1 + \frac{\Delta x_k}{\Delta x_{k-1}}\right)$ and $\beta_{1x} = \left(\frac{1}{4} + \frac{1}{2}\frac{\Delta x_k}{\Delta x_{k-1}} + \frac{1}{4}\frac{\Delta x_k^2}{\Delta x_{k-1}^2}\right)$

Similarly,

$$\overline{L^{k+1}_{gy}} = \frac{\int_{\frac{\Delta x_k}{2}}^{\left(\frac{\Delta x_k}{2}+\Delta x_{k+1}\right)} L^k_{gy}(x)\,dx}{\int_{\frac{\Delta x_k}{2}}^{\left(\frac{\Delta x_k}{2}+\Delta x_{k+1}\right)} dx} = \frac{1}{\Delta x_{k+1}} \int_{\frac{\Delta x_k}{2}}^{\left(\frac{\Delta x_k}{2}+\Delta x_{k+1}\right)} L^k_{gy}(x)\,dx$$

$$\Rightarrow \overline{L^{k+1}_{gy}} = \overline{L^k_{gy}} + \frac{b^k_{gy1}}{2}\alpha_{2x} + 3b^k_{gy2}\beta_{2x} \quad (20)$$

where $\alpha_{2x} = \left(1 + \frac{\Delta x_k}{\Delta x_{k+1}}\right)$ and $\beta_{2x} = \left(\frac{1}{4} + \frac{1}{2}\frac{\Delta x_k}{\Delta x_{k+1}} + \frac{1}{4}\frac{\Delta x_k^2}{\Delta x_{k+1}^2}\right)$

Solving Eqs. (19) and (20),

$$\left.\begin{aligned} b^k_{gy1} &= 2\frac{\left(\overline{L^{k+1}_{gy}} - \overline{L^k_{gy}}\right)\beta_{1x} - \left(\overline{L^{k-1}_{gy}} - \overline{L^k_{gy}}\right)\beta_{2x}}{(\alpha_{1x}\beta_{2x} + \alpha_{2x}\beta_{1x})} \\ b^k_{gy2} &= \frac{\left(\overline{L^{k+1}_{gy}} - \overline{L^k_{gy}}\right)\alpha_{1x} + \left(\overline{L^{k-1}_{gy}} - \overline{L^k_{gy}}\right)\alpha_{2x}}{3(\alpha_{1x}\beta_{2x} + \alpha_{2x}\beta_{1x})} \end{aligned}\right\} \left(\text{similar for } b^k_{gx1},\ b^k_{gx2},\ b^k_{gz1},\ b^k_{gz2}\right) \quad (21)$$

Now, from the definition of L^k_{gyxi} in Eq. (8.1),

$$L^k_{gyx1} = \frac{\int_{-\frac{\Delta x_k}{2}}^{\frac{\Delta x_k}{2}} L^k_{gy}(x) f_1(x)\,dx}{\int_{-\frac{\Delta x_k}{2}}^{\frac{\Delta x_k}{2}} dx}$$

$$= \frac{1}{\Delta x_k}\int_{-\frac{\Delta x_k}{2}}^{\frac{\Delta x_k}{2}} \left\{\overline{L^k_{gy}} + b^k_{gy1}\left(\frac{x}{\Delta x_k}\right) + b^k_{gy2}\left(3\left(\frac{x}{\Delta x_k}\right)^2 - \frac{1}{4}\right)\right\}\left(\frac{x}{\Delta x_k}\right) dx$$

$$= \frac{b^k_{gy1}}{12} \quad (22.1)$$

Similarly, from the definition of L^k_{gzxi} in Eq. (8.1),

$$L^k_{gzx1} = \frac{b^k_{gz1}}{12} \quad (22.2)$$

Therefore, $L^k_{gx1} = \frac{1}{\Delta y_k}L^k_{gyx1} + \frac{1}{\Delta z_k}L^k_{gzx1} = \frac{1}{12}\left(\frac{b^k_{gy1}}{\Delta y_k} + \frac{b^k_{gz1}}{\Delta z_k}\right)$ (from Eqs. (22.1) and (22.2))

$$= \frac{1}{12}\left(\frac{2}{\Delta y_k}\frac{\left(\overline{L^{k+1}_{gy}} - \overline{L^k_{gy}}\right)\beta_{1x} - \left(\overline{L^{k-1}_{gy}} - \overline{L^k_{gy}}\right)\beta_{2x}}{(\alpha_{1x}\beta_{2x} + \alpha_{2x}\beta_{1x})}\right.$$

$$\left. + \frac{2}{\Delta z_k}\frac{\left(\overline{L^{k+1}_{gz}} - \overline{L^k_{gz}}\right)\beta_{1x} - \left(\overline{L^{k-1}_{gz}} - \overline{L^k_{gz}}\right)\beta_{2x}}{(\alpha_{1x}\beta_{2x} + \alpha_{2x}\beta_{1x})}\right) \quad \text{(from Eq. 21)}$$

$$\Rightarrow L^k_{gx1} = \frac{\left(\begin{aligned} &\left(\frac{J^{k+1}_{gy+,out} - J^{k+1}_{gy+,in} - J^{k+1}_{gy-,in} + J^{k+1}_{gy-,out}}{\Delta y_k} + \frac{J^{k+1}_{gz+,out} - J^{k+1}_{gz+,in} - J^{k+1}_{gz-,in} + J^{k+1}_{gz-,out}}{\Delta z_k}\right)\beta_{1x} \\ &-\left(\frac{J^{k-1}_{gy+,out} - J^{k-1}_{gy+,in} - J^{k-1}_{gy-,in} + J^{k-1}_{gy-,out}}{\Delta y_k} + \frac{J^{k-1}_{gz+,out} - J^{k-1}_{gz+,in} - J^{k-1}_{gz-,in} + J^{k-1}_{gz-,out}}{\Delta z_k}\right)\beta_{2x} \\ &+\left(\frac{-J^k_{gy+,out} + J^k_{gy+,in} + J^k_{gy-,in} - J^k_{gy-,out}}{\Delta y_k} + \frac{-J^k_{gz+,out} + J^k_{gz+,in} + J^k_{gz-,in} - J^k_{gz-,out}}{\Delta z_k}\right)(\beta_{1x} - \beta_{2x}) \end{aligned}\right)}{6(\alpha_{1x}\beta_{2x} + \alpha_{2x}\beta_{1x})} \quad (23)$$

Likewise,

$$\Rightarrow L^k_{gx2}=\frac{\left(\begin{array}{l}\left(\frac{J^{k+1}_{gy+,out}-J^{k+1}_{gy+,in}-J^{k+1}_{gy-,in}+J^{k+1}_{gy-,out}}{\Delta y_k}+\frac{J^{k+1}_{gz+,out}-J^{k+1}_{gz+,in}-J^{k+1}_{gz-,in}+J^{k+1}_{gz-,out}}{\Delta z_k}\right)\alpha_{1x}\\+\left(\frac{J^{k-1}_{gy+,out}-J^{k-1}_{gy+,in}-J^{k-1}_{gy-,in}+J^{k-1}_{gy-,out}}{\Delta y_k}+\frac{J^{k-1}_{gz+,out}-J^{k-1}_{gz+,in}-J^{k-1}_{gz-,in}+J^{k-1}_{gz-,out}}{\Delta z_k}\right)\alpha_{2x}\\+\left(\frac{-J^{k}_{gy+,out}+J^{k}_{gy+,in}+J^{k}_{gy-,in}-J^{k}_{gy-,out}}{\Delta y_k}+\frac{-J^{k}_{gz+,out}+J^{k}_{gz+,in}+J^{k}_{gz-,in}-J^{k}_{gz-,out}}{\Delta z_k}\right)(\alpha_{1x}+\alpha_{2x})\end{array}\right)}{60(\alpha_{1x}\beta_{2x}+\alpha_{2x}\beta_{1x})} \tag{24}$$

Derivations of other leakage moments are quite similar.

For nodes situated at the left side boundary of reactor, there is no neighbouring node on their left side (no $(k-1)$th node existing). Hence, the leakage expansion coefficients b^k_{gy1} and b^k_{gy2} are determined by calculating average y-directed leakage of $(k+1)$ th and $(k+2)$ th node. Therefore, Eq. (19) is modified as

$$\overline{L^{k+2}_{gy}}=\frac{\int_{\left(\frac{\Delta x_k}{2}+\Delta x_{k+1}\right)}^{\left(\frac{\Delta x_k}{2}+\Delta x_{k+1}+\Delta x_{k+2}\right)}L^k_{gy}(x)\,dx}{\int_{\left(\frac{\Delta x_k}{2}+\Delta x_{k+1}\right)}^{\left(\frac{\Delta x_k}{2}+\Delta x_{k+1}+\Delta x_{k+2}\right)}dx}=\frac{1}{\Delta x_{k+2}}\int_{\left(\frac{\Delta x_k}{2}+\Delta x_{k+1}\right)}^{\left(\frac{\Delta x_k}{2}+\Delta x_{k+1}+\Delta x_{k+2}\right)}$$

$$L^k_{gy}(x)\,dx\ \Rightarrow\ \overline{L^{k+2}_{gy}}=\overline{L^k_{gy}}-\frac{b^k_{gy1}}{2}\alpha^L_{1x}+3b^k_{gy2}\beta^L_{1x} \tag{25}$$

where $\alpha^L_{1x}=-\left(1+\frac{\Delta x_k}{\Delta x_{k+2}}+\frac{2\Delta x_{k+1}}{\Delta x_{k+2}}\right)$ and $\beta^L_{1x}=\left(\frac{\Delta x_k^2}{4\Delta x_{k+2}^2}+\frac{\Delta x_k\Delta x_{k+1}}{\Delta x_{k+2}^2}+\frac{\Delta x_k}{2\Delta x_{k+2}}+\frac{\Delta x_{k+1}}{\Delta x_{k+2}}+\frac{\Delta x_{k+1}^2}{\Delta x_{k+2}^2}+\frac{1}{4}\right)$

Equations of leakage moments for these nodes are same as in Eqs. (23) and (24), but α_{1x} and β_{1x} will be replaced by α^L_{1x} and β^L_{1x}.

Similarly, for nodes situated at the right side boundary of reactor, there is no neighbouring node on their right side (no $(k+1)$th node existing). Hence, the leakage expansion coefficients b^k_{gy1} and b^k_{gy2} are determined by calculating average y-directed leakage of $(k-1)$th and $(k-2)$th node. Therefore, Eq. (20) is modified as

$$\overline{L^{k-2}_{gy}}=\frac{\int_{-\left(\frac{\Delta x_k}{2}+\Delta x_{k-1}\right)}^{-\left(\frac{\Delta x_k}{2}+\Delta x_{k-1}+\Delta x_{k-2}\right)}L^k_{gy}(x)\,dx}{\int_{-\left(\frac{\Delta x_k}{2}+\Delta x_{k-1}\right)}^{-\left(\frac{\Delta x_k}{2}+\Delta x_{k-1}+\Delta x_{k-2}\right)}dx}=\frac{1}{\Delta x_{k-2}}\int_{\left(\frac{\Delta x_k}{2}+\Delta x_{k+1}\right)}^{\left(\frac{\Delta x_k}{2}+\Delta x_{k+1}+\Delta x_{k+2}\right)}$$

$$L^k_{gy}(x)\,dx\ \Rightarrow\ \overline{L^{k-2}_{gy}}=\overline{L^k_{gy}}+\frac{b^k_{gy1}}{2}\alpha^R_{2x}+3b^k_{gy2}\beta^R_{2x} \tag{26}$$

where $\alpha^R_{2x}=-\left(1+\frac{\Delta x_k}{\Delta x_{k-2}}+\frac{2\Delta x_{k-1}}{\Delta x_{k-2}}\right)$ and $\beta^R_{2x}=\left(\frac{\Delta x_k^2}{4\Delta x_{k-2}^2}+\frac{\Delta x_k\Delta x_{k-1}}{\Delta x_{k-2}^2}+\frac{\Delta x_k}{2\Delta x_{k-2}}+\frac{\Delta x_{k-1}}{\Delta x_{k-2}}+\frac{\Delta x_{k-1}^2}{\Delta x_{k-2}^2}+\frac{1}{4}\right)$.

Equations of leakage moments for these nodes are same as in Eqs. (23) and (24), but α_{2x} and β_{2x} will be replaced by α^R_{2x} and β^R_{2x}.

4. Discontinuity factor: importance and incorporation in calculation

Solving diffusion equation after obtaining homogenized parameters via spatial homogenization and group condensation, as discussed in introduction, is not always equivalent to solving neutron transport equation for a heterogeneous reactor. Due to preservation of reaction rate only, as adopted in conventional homogenization methods, homogenization error in HAFAS BWR benchmark problem was reported in literature (Smith, 1986). Discontinuity factor (or sometimes called assembly discontinuity factor or ADF), as defined below, is introduced by K. S. Smith to preserve both reaction rate and surface averaged current simultaneously and thereby avoid this homogenization error.

$$f^k_{gs}=\frac{\phi^k_{gs,het}}{\phi^k_{gs,hom}} \tag{27}$$

where f^k_{gs} is discontinuity factor for gth energy group and sth surface of kth node or assembly, $\phi^k_{gs,het}$ is heterogeneous flux calculated by transport theory in detailed heterogeneous geometry and averaged over the surface s and $\phi^k_{gs,hom}$ is homogeneous flux calculated by diffusion theory and averaged over the same surface s. In this equation, homogeneous flux continuity condition is relaxed and heterogeneous flux continuity condition is imposed across the interface between two adjacent nodes. Discontinuity factors are calculated in transport theory based lattice code. If the assembly has heterogeneities like fuel pins of different enrichment, burnable absorber pins, presence of control blade near to assembly boundary etc., the discontinuity factors must be taken into account while solving diffusion equation. In NEMSQR, these factors are included in the calculation through following equation which gives a relation between outgoing and incoming partial currents through a surface $u\pm$ of kth assembly and incoming partial current through the same surface $u\mp$ of $(k\pm1)$th assembly.

$$J^{k\pm1}_{gu\mp,in}=J^k_{gu\pm,out}\left\{\frac{1}{2}\left(\frac{f^k_{gu\pm}}{f^{k\pm1}_{gu\mp}}+1\right)\right\}+J^k_{gu\pm,in}\left\{\frac{1}{2}\left(\frac{f^k_{gu\pm}}{f^{k\pm1}_{gu\mp}}-1\right)\right\};\quad u=x,y,z \tag{28}$$

Symbols are indicated in Fig. 2. By default, discontinuity factors are 1 which makes Eq. (28) as $J^{k\pm1}_{gu\mp,in}=J^k_{gu\pm,out}$ and whenever there is a scope to calculate them, prior to diffusion calculation, by lattice code, then those calculated values are used in Eq. (28). In DYN3D, a code for three dimensional simulation of steady state and transients in light water reactor cores with quadratic and hexagonal fuel assemblies, similar relation is reported to be used (Grundmann et al., 2005).

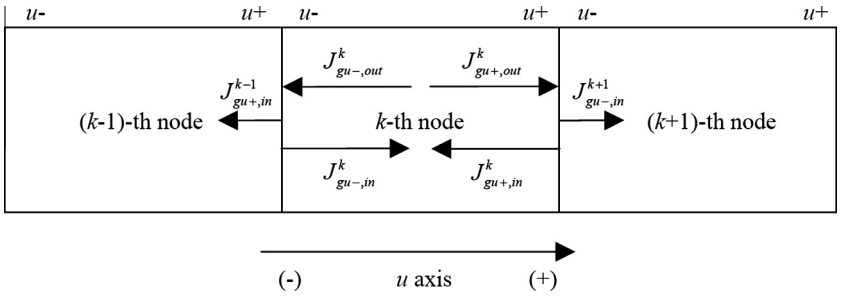

Fig. 2. Illustration of symbols used in Eq. (28); $(k-1)$, k and $(k+1)$ are node indices, g is energy group index, $+u$ is positive u directed surface and $-u$ is negative u directed surface of each node, f s' are discontinuity factors of respective energy groups and nodal surfaces, $J^{k\pm1}_{gu\mp,in}$ is gth group incoming current passing through $u\mp$ surfaces of $(k\pm1)$th node, $J^k_{gu\pm,out}$ and $J^k_{gu\pm,in}$ are gth group outgoing and incoming currents passing through $u\pm$ surfaces of kth node respectively.

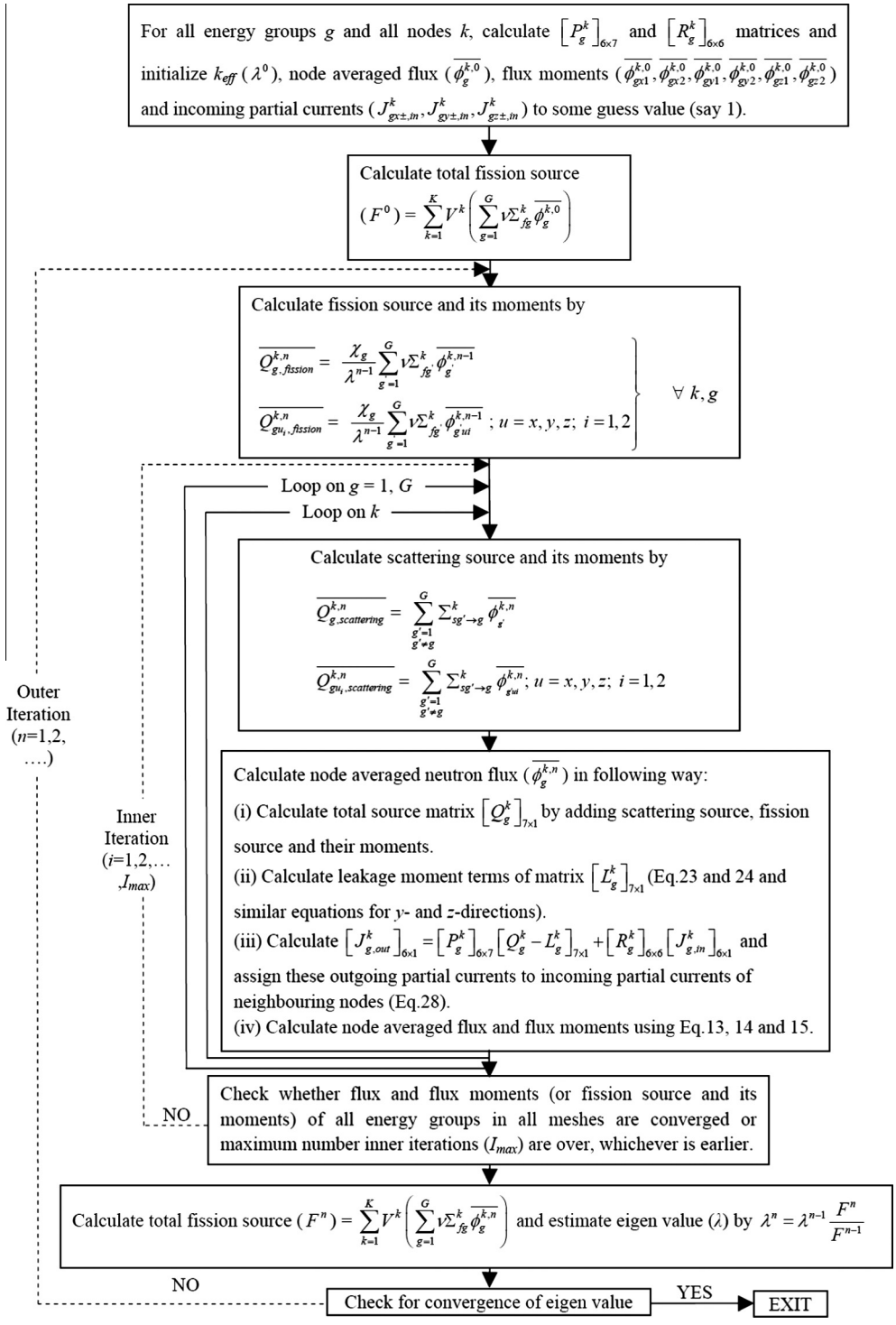

Fig. 3. Flowchart of nodal method based diffusion theory code NEMSQR.

5. Calculation of k_{eff}-value, neutron flux and fission power distribution

Iteration technique is used to solve steady state neutron diffusion equation (Eq. (1)) and obtain multiplication factor or k_{eff}-value, neutron flux and fission power distribution. There are two types of iteration; inner and outer. At the beginning of outer iteration, fission source is calculated and then keeping this fission source constant, nodal flux is calculated in inner iteration which continues until the flux converges or number of inner iteration reaches a cut-off. Now, after coming out of inner iteration, k_{eff} value is calculated and when this k_{eff} converges to a specified extent, outer iteration terminates. Flowchart of the calculation is given in Fig. 3. and steps are briefly described here.

(i) $\left[P_g^k\right]_{6\times7}$ and $\left[R_g^k\right]_{6\times6}$ matrices, as given in Eq. (17), are calculated for all nodes k and all energy groups g. Since matrix elements are dependent on some constant quantities like

homogenized removal cross section, diffusion coefficient and dimension of node in x-, y- and $z-$ directions, this calculation is performed only once before the iteration starts.

(ii) Some guess value (say 1) of k_{eff} (λ^0), flux ($\overline{\phi_g^{k,0}}$), flux moments $\left(\overline{\phi_{gx1}^{k,0}}, \overline{\phi_{gx2}^{k,0}}, \overline{\phi_{gy1}^{k,0}}, \overline{\phi_{gy2}^{k,0}}, \overline{\phi_{gz1}^{k,0}}, \overline{\phi_{gz2}^{k,0}}\right)$ and incoming partial currents $\left(J_{gx\pm,in}^k, J_{gy\pm,in}^k, J_{gz\pm,in}^k\right)$ in all nodes k for all energy groups g is taken ("0" in superscript indicates values before the outer iteration starts). Total fission source (F^0) summed over all nodes k and all energy groups g is calculated.

$$F^0 = \sum_{k=1}^{K} V^k \left(\sum_{g=1}^{G} \nu \Sigma_{fg}^k \overline{\phi_g^{k,0}} \right) \tag{29}$$

(iii) At the beginning of outer iteration n, fission source and its moments, as defined below, is calculated from flux, flux moment and k_{eff} values obtained in previous outer iteration $(n-1)$ (or, it will be guess value if it is the first outer iteration i.e. $n = 1$) for all nodes k and all energy groups g.

$$\left.\begin{aligned} \overline{Q_{g,fission}^{k,n}} &= \frac{\chi_g}{\lambda^{n-1}} \sum_{g'=1}^{G} \nu \Sigma_{fg'}^k \overline{\phi_{g'}^{k,n-1}} \\ \overline{Q_{gu_i,fission}^{k,n}} &= \frac{\chi_g}{\lambda^{n-1}} \sum_{g'=1}^{G} \nu \Sigma_{fg'}^k \overline{\phi_{g'ui}^{k,n-1}}; \quad u = x,y,z; \;\; i = 1,2 \end{aligned}\right\} \forall k, g \tag{30}$$

(iv) Thereafter inner iteration starts. Scattering source and its moments for kth node and gth energy group, as given below, are calculated with latest flux and flux moment values.

$$\left.\begin{aligned} \overline{Q_{g,scattering}^{k,n}} &= \sum_{\substack{g'=1 \\ g' \neq g}}^{G} \sum_{1^{sg' \to g}}^{k} \overline{\phi_{g'}^{k,n}} \\ \overline{Q_{gu_i,scattering}^{k,n}} &= \sum_{\substack{g'=1 \\ g' \neq g}}^{G} \sum_{1^{sg' \to g}}^{k} \overline{\phi_{g'ui}^{k,n}}; \quad u = x,y,z; \;\; i = 1,2 \end{aligned}\right\} \tag{31}$$

Scattering source, fission source and their moments, calculated for kth node and gth energy group, makes total source matrix $\left[Q_g^k\right]_{7\times1}$ in Eq. (17).

(v) Leakage moment terms of matrix $\left[L_g^k\right]_{7\times1}$ for kth node and gth energy group, as defined in Eqs. (23) and (24) (similar equations are applicable for y- and z-directions), are calculated using latest incoming and outgoing partial currents $\left(J_{gx\pm,out}^k, J_{gy\pm,out}^k, J_{gz\pm,out}^k\right)$.

(vi) Finally, outgoing partial current matrix $\left[J_{g,out}^k\right]_{6\times1}$ for kth node and gth energy group are calculated using $\left[P_g^k\right]_{6\times7}$, $\left[R_g^k\right]_{6\times6}$ obtained in step (i), $\left[Q_g^k\right]_{7\times1}$ obtained in step (iv), $\left[L_g^k\right]_{7\times1}$ obtained in step (v) and latest incoming partial currents of matrix $\left[J_{g,in}^k\right]_{6\times1}$ (Eq. (17)). These outgoing partial currents are assigned to the incoming partial currents of neighbouring nodes through respective surfaces (Eq. (28)). New flux and flux moment values are derived from partial currents using Eqs. (13,14,15) (similar equations are applicable for y- and z-directions).

(vii) Steps (iv)–(vi) are repeated for all nodes and all energy groups, keeping fission source and its moments, calculated in step (iii) constant. One inner iteration is completed after sweeping over all nodes and all energy groups. Inner iteration continues until the convergence criterion on flux (and its moments for tighter convergence) or in equivalent case, on fission source (and its moments) is satisfied or number of inner iteration reaches a preset value.

(viii) As soon as inner iteration terminates, fission source for nth outer iteration (F^n) summed over all nodes k and all energy groups g is calculated.

$$F^n = \sum_{k=1}^{K} V^k \left(\sum_{g=1}^{G} \nu \Sigma_{fg}^k \phi_g^{k,n} \right) \tag{32}$$

A new k_{eff} value is calculated from k_{eff} value (λ^{n-1}) and fission source (F^{n-1}) obtained in previous outer iteration $(n-1)$ (or, it will be the values mentioned in step (ii) if it is the first outer iteration i.e. $n = 1$) and fission source obtained in present outer iteration n (F^n).

$$\lambda^n = \lambda^{n-1} \frac{F^n}{F^{n-1}} \tag{33}$$

(ix) Outer iteration terminates when the convergence criterion on k_{eff} value is satisfied.

(x) Latest flux value, obtained from step (vi) after both inner and outer iterations are over, is scaled according to reactor power. One way of finding out the scale factor is to calculate total fission source by using the flux value (which is not scaled) obtained from nodal method and equate it with the fission source for the given reactor power (Fission source = $\nu \times 3.1 \times 10^{16} \times$ Reactor power (MW) where ν is average number neutrons released per fission reaction). Once neutron flux is obtained, fission power distribution can be calculated by multiplying macroscopic fission cross section with flux and volume of each node and then normalizing the product to reactor power.

6. Calculation of adjoint neutron flux and integral kinetics parameters

Solving only space dependent diffusion equation is not sufficient in case of studying reactor dynamics under any reactivity transient event. In such cases, neutron space time kinetics equations are solved by calculating shape function and some integral kinetics parameters from space dependent diffusion equation in larger time interval and then using these calculated kinetics parameter values, amplitude factor is calculated from point kinetics equation in smaller time interval. In a view to develop a space time kinetics code in future, NEMSQR is made capable to calculate integral kinetics parameters which include effective delayed neutron fraction and prompt neutron lifetime (or generation time). For the calculation of these parameters, steady state regular flux diffusion equation (Eq. (34.1), same as Eq. (1)) and adjoint flux diffusion equation (Eq. (34.2)), as given below, are considered.

$$\begin{aligned} &-\nabla D_g^k . \nabla \phi_g^k(x,y,z) + \sum_{rg}^{k} \phi_g^k(x,y,z) \\ &= \frac{\chi_g}{\lambda} \sum_{g'=1}^{G} \nu \sum_{fg'}^{k} \phi_{g'}^k(x,y,z) + \sum_{\substack{g'=1 \\ g' \neq g}}^{G} \sum_{sg' \to g}^{k} \phi_{g'}^k(x,y,z) \end{aligned} \tag{34.1}$$

$$\begin{aligned} &-\nabla D_g^k . \nabla \phi_g^{k\dagger}(x,y,z) + \sum_{rg}^{k} \phi_g^{k\dagger}(x,y,z) \\ &= \frac{\nu \sum_{fg}^{k}}{\lambda} \sum_{g'=1}^{G} \chi_{g'} \phi_{g'}^{k\dagger}(x,y,z) + \sum_{\substack{g'=1 \\ g' \neq g}}^{G} \sum_{sg \to g'}^{k} \phi_{g'}^{k\dagger}(x,y,z) \end{aligned} \tag{34.2}$$

$\phi_g^k(x,y,z)$ and $\phi_g^{k\dagger}(x,y,z)$ are called regular and adjoint flux respectively. After calculating both of them, effective delayed neutron fraction (β_{eff}) and prompt neutron lifetime (l) (or generation time Λ) are calculated by using following equations.

$$\left.\begin{aligned}\beta_{eff,i} &= \frac{\sum_k \left(\sum_{g=1}^{G} \chi_{dg}\phi_g^{k\dagger}\right)\times\left(\sum_{g=1}^{G} \nu\Sigma_{fg}^{k}\phi_g^{k}\right)\times V_k}{\sum_k \left(\sum_{g=1}^{G} \chi_{g}\phi_g^{k\dagger}\right)\times\left(\sum_{g=1}^{G} \nu\Sigma_{fg}^{k}\phi_g^{k}\right)\times V_k}\\ \beta_{eff} &= \sum_{i=1}^{G_d}\beta_{eff,i}\end{aligned}\right\} \tag{35}$$

$$\left.\begin{aligned}\Lambda &= \frac{\sum_k \left(\sum_{g=1}^{G} \phi_g^{k\dagger}\frac{1}{v_g}\phi_g^{k}\right)\times V_k}{\sum_k \left(\sum_{g=1}^{G} \chi_{g}\phi_g^{k\dagger}\right)\times\left(\sum_{g=1}^{G} \nu\Sigma_{fg}^{k}\phi_g^{k}\right)\times V_k}\\ l &= k_{eff}\Lambda\end{aligned}\right\} \tag{36}$$

Method of solution for regular flux diffusion equation is described in Section 5. For adjoint flux diffusion equation, method of solution is same only with a difference in Eqs. (30) and (31) and hence these two equations are modified as following.

$$\left.\begin{aligned}\overline{Q_{g,fission}^{k,n}} &= \frac{\nu\Sigma_{fg}^{k}}{\lambda^{n-1}}\sum_{g'=1}^{G}\chi_{g\prime}\overline{\phi_{g'}^{k,n-1,\dagger}}\\ \overline{Q_{gu_i fission}^{k,n}} &= \frac{\nu\Sigma_{fg}^{k}}{\lambda^{n-1}}\sum_{g'=1}^{G}\chi_{g\prime}\overline{\phi_{g'ui}^{k,n-1,\dagger}};\quad u=x,y,z;\ \ i=1,2\end{aligned}\right\}\forall k,g \tag{37}$$

$$\left.\overline{Q_{g,scattering}^{k,n}} = \sum_{\substack{g'=1\\ g'\neq g}}^{G}\sum_{sg\to g'}^{k}\overline{\phi_{g'}^{k,n,\dagger}};\quad u=x,y,z;\ \ i=1,2\right\} \tag{38}$$

One more difference is that the scattering source terms of gth energy group in Eq. (38) involve neutron fluxes of lower energy group g' (in most of the scattering cases except up-scattering, $g' < g$), which will be not known to us by that time if we start the iteration process from highest energy group and continue towards lowest energy group like the regular flux diffusion equation. Therefore, the iteration process for adjoint flux diffusion equation starts from lowest energy group and proceeds towards higher energy groups.

7. Calculation of subcritical count in presence of external neutron source

Nuclear reactors are sometimes required to be shutdown due to refueling, maintenance of system components involved in reactor operation and various other jobs. Response of neutron detectors, which helps us to operate the reactor by showing the response of neutrons in terms of neutronic power, starts decreasing as soon as the reactor is shutdown or made subcritical and continues to decrease unless there is any neutron source in core. If neutron source is present in terms of some external source or photo neutron source, detector response first decreases after shutdown and then attains a saturation value proportional to $S/(1-k_{eff})$ where S is neutron source strength. The code NEMSQR is capable to find out the detector response or subcritical count in presence of external neutron source. Method of calculation is same as described in Section 5 with a difference that credit of λ is not taken in this case (by omitting λ from all relevant expressions or setting it equal to 1 and not updating it throughout the calculation). Iteration terminates when subcritical count converges to the extent set by user. The results of this module are yet to be validated by modeling a suitable problem.

8. Results and discussion

8.1. Calculation of k_{eff}-value, neutron flux and fission power distribution

Three static benchmark problems are selected to validate the k_{eff}, neutron flux and fission power distribution calculation of code NEMSQR. First problem is a three dimensional IAEA PWR benchmark problem. Second one is static version of a three dimensional LRA BWR kinetics benchmark problem and third one is a three dimensional LMFBR benchmark problem which is a simplified model of MARK I core design of SNR 300 prototype LMFBR. In calculation, convergence criterion of 1.0×10^{-5} for fission source in each node and 1.0×10^{-7} for eigenvalue are taken. Maximum number of inner iterations is restricted to one per outer iteration. Full core calculation is carried out with incoming current zero condition applied at outermost boundary of core though quarter core calculation (since all three benchmark cores are quarter symmetric) with reflective boundary condition at symmetry boundary in addition to incoming current zero condition at outermost core boundary could have been done. Power distribution is calculated by setting average power per assembly to 1.0 KW. Accuracy of the code is determined by the percent errors ε_λ and ε_p^i for eigenvalue (λ) and assembly averaged power (P^i) distribution respectively.

Horizontal and vertical cross sections of benchmark reactor cores are generated by DISLIN, a high level plotting library (Michels, 1997). Description of the benchmark problems and their results are following.

8.1.1. 3D IAEA two neutron energy group PWR benchmark problem

The 3D IAEA PWR benchmark problem was introduced in 1971 by Micheelson and Neltrup (Micheelson and Neltrup, 1973) and later included in ANL-7416 (BSS-11, page no. 277 of ANL-7416, supplementary 2, June, 1977). In the problem, reactor core consists of 177 fuel assemblies including 108 type-I fuel assemblies (Fuel 1), 56 type-II fuel assemblies (Fuel 2), 15 rodded fuel assemblies (Fuel 2 + Rod) out of which 9 are fully rodded and 4 are partially rodded fuel assemblies. The quarter symmetric core is surrounded by 64 reflector assemblies both in axial and radial directions. Reflector elements at top of the rodded assemblies (Reflector + Rod) are different from rest of the reflector elements (Reflector). All assemblies are arranged in a square lattice of pitch 20 cm. Active height of a fuel assembly is 340 cm. Thickness of both axial and radial reflector is 20 cm. Figs. 4 and 5 depict horizontal and vertical cross sections of full reactor core respectively. Two group homogenized lattice parameters of different materials of the core, used in the calculation, are given in ANL-7416. Fission spectrum is taken as 1.0 (χ_1) and 0.0 (χ_2).

The calculation is performed for two different spatial meshes to show the dependence of mesh size on results. The coarse mesh solution (i.e. $20\times20\times20$) uses a 20 cm spatial mesh both in radial as well as axial directions whereas the fine mesh solution (i.e. $10\times10\times20(10)$) uses a 10 cm radial mesh and a 20 cm axial mesh except in the axial reflectors where a 10 cm axial mesh is used. In Fig. 6, radial power distribution of quarter core, k_{eff} value and their relative errors, as obtained from NEMSQR for fine mesh structure, are presented along with reference value. Reference k_{eff} value and power distribution are taken from benchmark solution given by Finnemann (11-A1-3, page no. 373, ANL-7416, supplementary 2, June, 1977) for $10\times10\times20(10)$ mesh structure using nodal method based code IQS-BOX where flux is expanded in each node up to fifth order. k_{eff} value for coarse mesh is 1.0296 and for fine mesh is 1.0293 while the reference value is 1.02904. Therefore, accuracy of solution increases with decrease in mesh size.

8.1.2. 3D LRA two neutron energy group BWR benchmark problem

The 3D LRA BWR benchmark problem was introduced by Langenbuch and Werner in ANL-7416 (BSS-14, page no. 548 of ANL-7416, supplementary 2, June, 1977). Initial static part of this full core kinetics benchmark problem is considered here. BWR core of the problem consists of 312 fuel assemblies including 160 controlled fuel assemblies of type-I (Fuel 1 with rod), 36 uncontrolled fuel assemblies of type-I (Fuel 1 without rod), 112 controlled fuel assemblies of type-II (Fuel 2 with rod) and 4

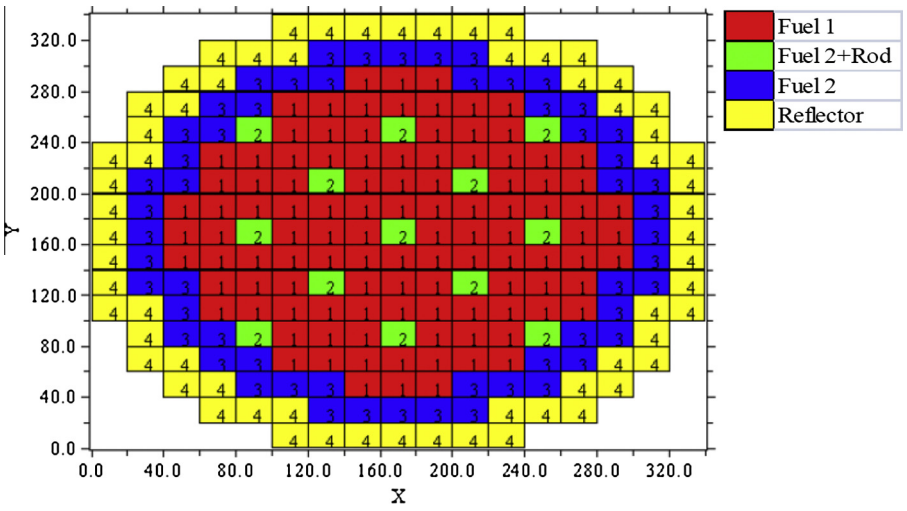

Fig. 4. Horizontal cross section of 3D IAEA two neutron energy group PWR benchmark core at 280.0 cm < z < 360.0 cm.

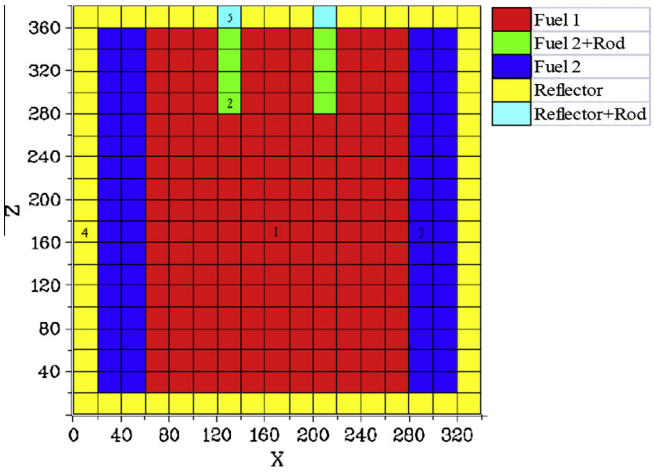

Fig. 5. Vertical cross section of 3D IAEA two neutron energy group PWR benchmark core at y = 120.0 cm or, y = 200.0 cm.

controlled fuel assemblies of type-II (Fuel 2 without rod). Like 3D IAEA PWR, this core has quarter symmetry and it is surrounded by 169 reflector assemblies both in axial and radial directions. Active height of a fuel assembly is 300 cm. Thickness of both axial and radial reflector is 30 cm. Horizontal cross section of full reactor core is given in Fig. 7. Two group homogenized lattice parameters of different materials of the core, used in the calculation, are given in ANL-7416. Fission spectrum is taken as 1.0 (χ_1) and 0.0 (χ_2) and average number of neutrons released per fission (ν) is 2.43.

The calculation is performed for three different spatial meshes. The coarse mesh solution (i.e. 15 × 15 × 25(15)) uses a 15 cm radial mesh and a 25 cm axial mesh except in the axial reflectors where a 15 cm axial mesh is used. The fine mesh solution (i.e. 7.5 × 7.5 × 12.5(7.5)) uses a 7.5 cm radial mesh and a 12.5 cm axial mesh except in the axial reflectors where a 7.5 cm axial mesh is used. The very fine mesh solution (i.e. 5 × 5 × 12.5(7.5)) uses a 5 cm radial mesh keeping axial mesh size same as in fine mesh. In Fig. 8, radial power distribution of quarter core, k_{eff} value and their relative errors, as obtained from NEMSQR for very fine mesh structure, are presented along with reference value. Reference k_{eff} value and power distribution are taken from solution given by Zerkle (page no. 114, Phd thesis by Zerkle, 1992) for 5 × 5 × 12.5(7.5) mesh structure using nodal method based code QUAGMIRE where quartic flux expansion with quadratic transverse leakage approximation in core and flat transverse leakage approximation in reflector is used. k_{eff} value for coarse mesh is 0.997437 which is improved quite significantly to 0.996786 for fine mesh and 0.996686 for very fine mesh where the reference value is 0.996381.

8.1.3. 3D LMFBR four neutron energy group benchmark problem

The 3D LMFBR benchmark problem was introduced by Buckel, Kuefner and Stehle in ANL-7416 (18-A2, page no. 810 of ANL-7416, supplementary 3, December, 1985). It is a challenging problem since it involves four energy group calculation. In the problem, quarter symmetric reactor core is divided into two concentric regions; inner and outer core region. Active height of these two core regions are 95 cm each. Reactor core is surrounded by blanket regions both radially (Radial blanket region) and axially (Axial blanket region). Thickness of radial blanket is variable and ranges from 29.7 cm to 72.55 cm (approx.) while axial blanket is 40 cm thick both at top and bottom. There are several locations in core where two types of absorber assemblies are placed. Absorber region of one type of assembly is extended from core top to bottom of top axial blanket and of second type of assembly is extended from core top to an elevation of height 87.5 cm. Rest of the region below absorber is filled with follower region. Fig. 9 depicts horizontal cross section of full reactor core. Four group homogenized lattice parameters of different materials of the core, used in the calculation, are given in (page no. 158–159, Phd thesis by Zerkle, 1992). Fission spectrum is taken as 0.768 (χ_1), 0.232 (χ_2), 0.0 (χ_3) and 0.0 (χ_4).

The calculation is performed for four different mesh sizes. First one is 5.4(8.1) × 5.4(8.1) × 9.5(10) which implies a mesh structure of a 5.4 cm radial mesh except at the end of radial blanket where a 8.1 cm radial mesh is used and a 9.5 cm axial mesh except in the axial blanket where a 10 cm axial mesh is used (38 × 38 × 18 mesh points for full core). k_{eff} value of the problem, as obtained from NEMSQR for the mesh structure explained above, is 1.015299 whereas the reference value is 1.013746 (ε_λ = 0.15). Reference k_{eff} value is taken from solution given by Finnemann (18-A2-3, page no. 821 of ANL-7416, supplementary 3, December, 1985) for the identical mesh structure using nodal method based code NEMBOX where quartic flux expansion is used. k_{eff} value from the code QUAGMIRE is 1.013695 for the same mesh structure, which may be considered to be the reference value for this benchmark problem (page no. 117, Phd thesis by Zerkle). Mesh sizes are reduced

						$\lambda_{cal} \rightarrow$	1.0293	
						$\lambda_{ref} \rightarrow$	1.02904	
						$\varepsilon_\lambda \rightarrow$	0.03	
0.0000	0.0000	0.0000	0.0000					
0.0000	0.0000	0.0000	0.0000					
0.00	0.00	0.00	0.00					
0.7846	0.7652	0.7143	0.0000	0.0000	0.0000			
0.7730	0.7530	0.7070	0.0000	0.0000	0.0000			
1.50	1.62	1.03	0.00	0.00	0.00			
0.9664	0.9802	1.0073	0.8707	0.6148	0.0000	0.0000		
0.9580	0.9740	0.9970	0.8640	0.6080	0.0000	0.0000		
0.88	0.64	1.03	0.78	1.12	0.00	0.00		
0.9586	1.0573	1.0929	0.9271	0.7094	0.5938	0.0000	0.0000	
0.9540	1.0550	1.0880	0.9230	0.6990	0.5970	0.0000	0.0000	
0.48	0.22	0.45	0.44	1.49	0.54	0.00	0.00	
0.6058	1.0762	1.1852	0.9770	0.4733	0.7079	0.6091	0.0000	
0.6100	1.0720	1.1810	0.9720	0.4750	0.6990	0.6080	0.0000	
0.69	0.39	0.36	0.51	0.36	1.27	0.18	0.00	
1.1950	1.2876	1.3095	1.1767	0.9749	0.9239	0.8644	0.0000	0.0000
1.1950	1.2920	1.3110	1.1790	0.9720	0.9230	0.8640	0.0000	0.0000
0.00	0.34	0.11	0.20	0.30	0.10	0.05	0.00	0.00
1.4233	1.4273	1.3618	1.3084	1.1838	1.0882	1.0015	0.7055	0.0000
1.4230	1.4320	1.3690	1.3110	1.1810	1.0880	0.9970	0.7070	0.0000
0.02	0.33	0.53	0.20	0.24	0.02	0.45	0.21	0.00
1.2807	1.3912	1.4274	1.2865	1.0734	1.0535	0.9750	0.7583	0.0000
1.2830	1.3980	1.4320	1.2910	1.0720	1.0550	0.9740	0.7530	0.0000
0.18	0.49	0.32	0.35	0.13	0.14	0.10	0.70	0.00
0.7205	1.2813	1.4219	1.1947	0.6047	0.9561	0.9610	0.7792	0.0000
0.7290	1.2830	1.4230	1.1950	0.6100	0.9530	0.9580	0.7730	0.0000
1.17	0.13	0.08	0.03	0.87	0.33	0.31	0.80	0.00

$P^i_{cal} \rightarrow$
$P^i_{ref} \rightarrow$
$\varepsilon^i_P \rightarrow$

Fig. 6. Comparison of quarter core power distribution, k_{eff} value as given by NEMSQR for 3D IAEA two neutron energy group PWR benchmark problem with those of code IQSBOX for identical mesh structure.

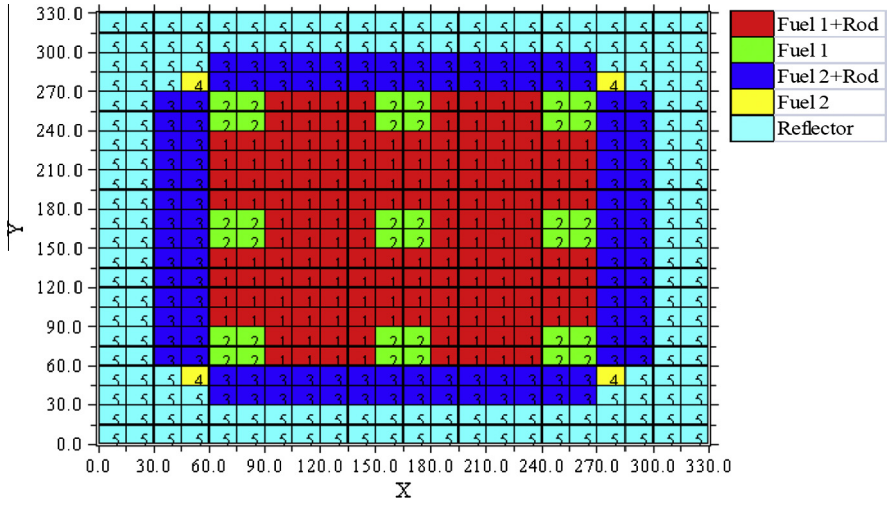

Fig. 7. Horizontal cross section of 3D LRA two neutron energy group BWR benchmark core at 30.0 cm < z < 330.0 cm.

further both in x–y and z directions and k_{eff} values so obtained are given in Table 1.

Relative percentage errors in the calculations of k_{eff} values and fission power (or neutron flux) distributions of all three problems are within 1–2% which confirms the accuracy of code. However, stability problem may be encountered if axial and radial mesh sizes are taken to be very different. As reported by Zerkley and in present case too, if axial mesh size is more than three times of radial mesh size, then such instability will be experienced. This problem will not exist if the mesh sizes in axial and radial direction are comparable.

8.2. Calculation of adjoint neutron flux and integral kinetics parameters

A benchmark problem (IAEA-TECDOC-643, 1992) is chosen to validate the calculation of adjoint neutron flux and integral kinetics parameters, implemented in the code NEMSQR. Following sec-

$\lambda_{cal} \rightarrow$	0.99669
$\lambda_{ref} \rightarrow$	0.99638
$\varepsilon_{\lambda} \rightarrow$	0.03

	0.9247	0.8682	0.8273	0.8529	0.9318	0.9699	0.8431	0.0000	0.0000
	0.9241	0.8671	0.8267	0.8527	0.9321	0.9711	0.8457	0.0000	0.0000
	0.0649	0.1269	0.0726	0.0235	0.0322	0.1236	0.3074	0.0000	0.0000
	1.4839	1.2846	1.1741	1.2215	1.4220	1.6767	1.6188	1.3247	0.0000
	1.4811	1.2811	1.1729	1.2212	1.4212	1.6787	1.6204	1.3271	0.0000
	0.1890	0.2732	0.1023	0.0246	0.0563	0.1191	0.0987	0.1808	0.0000
	1.6691	1.1544	0.9690	1.0234	1.3390	2.0520	2.1608	1.6189	0.8429
	1.6606	1.1510	0.9670	1.0225	1.3391	2.0499	2.1596	1.6204	0.8457
	0.5119	0.2954	0.2068	0.0880	0.0075	0.1024	0.0556	0.0926	0.3311
	1.3934	0.9442	0.7856	0.8452	1.1528	1.8537	2.0517	1.6765	0.9698
	1.3851	0.9401	0.7830	0.8436	1.1520	1.8512	2.0499	1.6787	0.9711
	0.5992	0.4361	0.3321	0.1897	0.0694	0.1350	0.0878	0.1311	0.1339
	0.7947	0.6756	0.6221	0.6815	0.8676	1.1526	1.3388	1.4217	0.9316
	0.7906	0.6706	0.6184	0.6784	0.8643	1.1520	1.3391	1.4212	0.9321
	0.5186	0.7456	0.5983	0.4570	0.3818	0.0521	0.0224	0.0352	0.0536
	0.5157	0.4947	0.4963	0.5564	0.6814	0.8450	1.0230	1.2210	0.8526
	0.5123	0.4907	0.4923	0.5527	0.6784	0.8436	1.0225	1.2212	0.8527
	0.6637	0.8152	0.8125	0.6694	0.4422	0.1660	0.0489	0.0164	0.0117
	0.4170	0.4110	0.4283	0.4963	0.6220	0.7853	0.9685	1.1736	0.8270
	0.4134	0.4070	0.4243	0.4923	0.6184	0.7830	0.9670	1.1729	0.8267
	0.8708	0.9828	0.9427	0.8125	0.5821	0.2937	0.1551	0.0597	0.0363
	0.4451	0.4044	0.4110	0.4947	0.6754	0.9438	1.1539	1.2840	0.8678
	0.4406	0.3998	0.4070	0.4907	0.6706	0.9401	1.1510	1.2811	0.8671
	1.0213	1.1506	0.9828	0.8152	0.7158	0.3936	0.2520	0.2264	0.0807
$P^i_{cal} \rightarrow$	0.6199	0.4452	0.4170	0.5157	0.7946	1.3930	1.6683	1.4832	0.9242
$P^i_{ref} \rightarrow$	0.6124	0.4406	0.4134	0.5123	0.7906	1.3851	1.6606	1.4811	0.9241
$\varepsilon^i_P \rightarrow$	1.2247	1.0440	0.8708	0.6637	0.5059	0.5704	0.4637	0.1418	0.0108

Fig. 8. Comparison of quarter core power distribution, k_{eff} value as given by NEMSQR for 3D LRA two neutron energy group BWR benchmark problem with those of code QUAGMIRE for identical mesh structure.

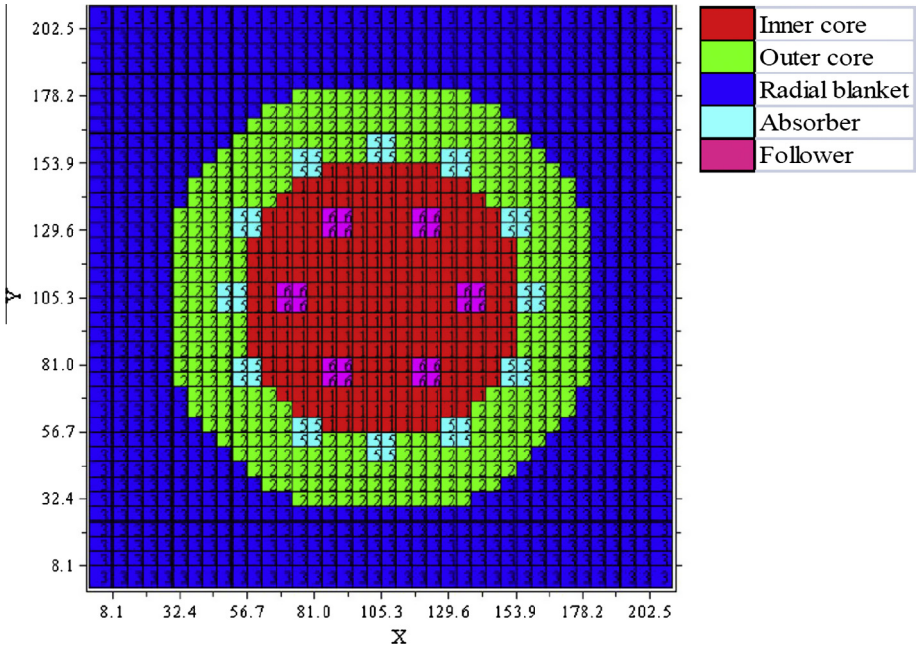

Fig. 9. Horizontal cross section of 3D four neutron energy group LMFBR benchmark core at 87.5 cm < z < 135.0 cm.

Table 1
k_{eff} Value of 3D LMFBR core for different mesh sizes.

Mesh size	Mesh points	k_{eff} Value
5.4(8.1) × 5.4(8.1) × 9.5(10)	38 × 38 × 18	1.015299
2.7(4.05) × 2.7(4.05) × 9.5(10)	76 × 76 × 18	1.014810
5.4(8.1) × 5.4(8.1) × 4.75(5)	38 × 38 × 36	1.014581
2.7(4.05) × 2.7(4.05) × 4.75 (5)	76 × 76 × 36	1.014107

tion gives a brief description of the problem and comparison of results of the code with benchmark values.

8.2.1. Safety related benchmark problem of IAEA-TECDOC-643

The problem is originally designed to assist the research reactor operators in addressing safety and licensing issues for research reactor core conversion from highly enriched uranium (HEU) to low enriched uranium (LEU). As a part of neutronic transient study discussed in the guidebook, prompt neutron generation time, prompt neutron lifetime and delayed neutron fraction of benchmark reactor core were calculated and hence the problem is chosen to validate NEMSQR. The benchmark reactor is a 10 MW_{th} pool type graphite reflected light water research reactor. Core map is shown in Fig. 10. Material numbers indicated in the figure are written within a parenthesis {} after the name of implied material appeared in text below. The core is similar to the problem discussed in IAEA-TECDOC-233 (IAEA-TECDOC-233, 1980) except the water filled central flux trap which is replaced in the present problem with a 77 mm × 81 mm aluminum block containing a square hole of 50 mm × 50 mm. Two types of core configuration are considered in the IAEA report. One is HEU core and another is LEU core. Since validation study is carried out on LEU core, information of LEU core is only given here. Fuel of LEU core is UAl_x-Al which comprises of 72% (% means wt.%) uranium and 28% aluminum. This uranium is made of 20% (i.e. 16.956 gm) U^{235} and 80% U^{238}. The reactor core, consisted of 21 (20 full and 2 half assembly) standard fuel assemblies (SFA) 2–4 numbered assemblies as indicated in Fig. 10, 4 control fuel assemblies (CFA) {5}, 8 graphite reflector assemblies {6} and 1 central flux trap {1}, is surrounded by 3 fuel element width (i.e. 24.3 cm in *X* direction and 23.1 cm in *Y* direction as shown in Fig. 10) of water reflector {7} in radial direction. All assemblies are of size 77 mm × 81 mm and active core height is 600 mm. Kinetics parameters are calculated for the core at BOC (Beginning Of Cycle) which has 8 SFAs of 5% burn up {2}, 6 SFAs of 25% burn up {3}, 7 (6 full and 2 half assembly) SFAs of 45% burn up {4} and 4 CFAs of 25% burn up {5}. Dimensions of SFA and CFA are shown in IAEA-TECDOC-643 (page no. 17). SFA is composed of 23 fuel plates of dimension 63 mm × 0.51 mm × 600 mm, cladded with 0.38 mm thick aluminum. Structure-wise CFA is similar to SFA except the fact that 3 fuel plates on each side of CFA are replaced with a control blade surrounded by 2 aluminum plates.

Calculations of adjoint neutron flux and integral kinetics parameters are carried out for three neutron energy groups with the help of one dimensional transport theory lattice code WIMSD4 (Askew et al., 1966), two dimensional transport theory lattice code TWOTRAN (Lathrop and Brinkley, 1970) and NEMSQR. The three energy groups formed are (i) Thermal (0–0.625 eV), (ii) Epithermal (0.625 eV to 0.821 MeV) and (iii) Fast (0.821–10.0 MeV). WIMSD4 and TWOTRAN codes in conjunction with 69 neutron energy group ENDF/B-VI cross section data library are used to generate three group homogenized macroscopic cross sections of each type of assembly, which are subsequently used as input to NEMSQR for adjoint neutron flux and integral kinetics parameters calculation. $1/v$ values used in the calculation are computed, weighting $1/v$ values by neutron fluxes of fine energy groups making up the three broad energy groups. $1/v$ values of the fine groups correspond to the mid-point energies of the groups. Total effective delayed neutron fraction and prompt neutron lifetime (or generation time Λ), as given by NEMSQR are 0.007252 and 42.58 μs (41.48 μs) respectively whereas the corresponding reference values are 0.007275 and 44.53 μs (43.74 μs) taken from solution given by Matos et. al. (page no. 18, IAEA-TECDOC-643, 1992) for 10 energy group structure using lattice level code EPRI-CELL and diffusion theory based code DIF2D. Effective multiplication factor, calculated by NEMSQR, is 1.02653 whereas the same as calculated by various organizations are 1.01796 (ANL, page no. 18, IAEA-TECDOC-643), 1.026385 (EIR, page no. 113, IAEA-TECDOC-643), 1.032 (OSGAE, page no. 537, IAEA-TECDOC-233), 1.05782 (JAERI, page no. 594, IAEA-TECDOC-233), 1.0394 (CEA, page no. 558, IAEA-TECDOC-233) and 1.03316 (CNEA, page no. 617, IAEA-TECDOC-233). Various spatial homogenization techniques adopted by different group causes the difference between multiplication factors.

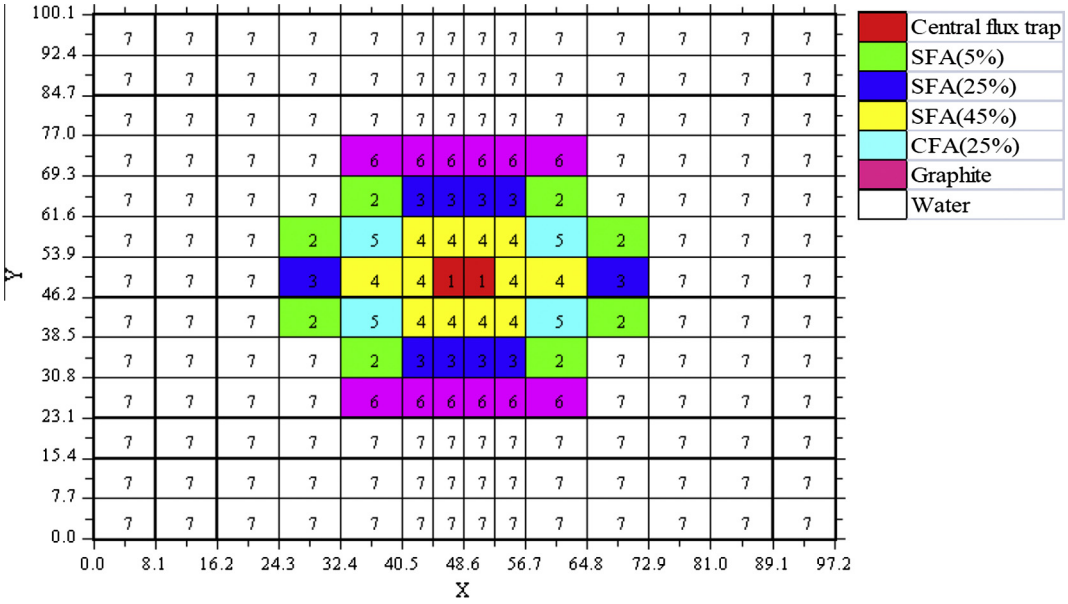

Fig. 10. Schematic horizontal cross-section of safety related benchmark core of IAEA-TECDOC-643 at BOC.

9. Conclusion

It is concluded that the nodal expansion method in its present form is adequate for the purpose of design calculation of research as well as power reactors. Results of benchmark problems clearly show that the error in k_{eff} value is less than 0.5 mk and in power distribution is less than 2%. This error can be reduced further by applying discontinuity factor, if its value is available, or reducing mesh size, which are already included in the code. Though acceleration scheme is not adopted in the calculation as the inherent feature of nodal method that one can take a mesh size equal to the size of an assembly helps to reduce computational time to a great extent as compared to finite difference method, the scheme will be included in future as an improvement over the existing code. NEMSQR is written only for static problem and there is a scope to modify it for reactivity transient analysis.

Acknowledgements

Authors would like to thank Shri R.C. Sharma, Head, RRSD and Dr. Kanchhi Singh, Head, RPNES, RRSD for their constant support and encouragement to carry out this work.

Appendix A

A.1. Matrix elements of Eq. (17)

Elements of $[A]_{6\times6}$, $[B]_{6\times7}$ and $[C]_{6\times6}$ matrices of Eq. (17) are given below.

$$a_{11}=a_{22}=\left(1+\frac{32D_g^k}{\Delta x_k}+\frac{120D_g^k}{\sum_{rg}^k\Delta x_k^2}+\frac{960D_g^{k2}}{\sum_{rg}^k\Delta x_k^3}+\frac{840D_g^{k2}}{\sum_{rg}^{k2}\Delta x_k^4}\right)$$

$$c_{11}=c_{22}=\left(1-\frac{32D_g^k}{\Delta x_k}+\frac{120D_g^k}{\sum_{rg}^k\Delta x_k^2}-\frac{960D_g^k}{\sum_{rg}^k\Delta x_k^3}+\frac{840D_g^{k2}}{\sum_{rg}^{k2}\Delta x_k^4}\right)$$

$$a_{12}=a_{21}=\left(\frac{8D_g^k}{\Delta x_k}+\frac{60D_g^k}{\sum_{rg}^k\Delta x_k^2}+\frac{720D_g^{k2}}{\sum_{rg}^k\Delta x_k^3}+\frac{840D_g^{k2}}{\sum_{rg}^{k2}\Delta x_k^4}\right)$$

$$c_{12}=c_{21}=\left(-\frac{8D_g^k}{\Delta x_k}+\frac{60D_g^k}{\sum_{rg}^k\Delta x_{k2}}-\frac{720D_g^{k2}}{\sum_{rg}^k\Delta x_{k3}}+\frac{840D_g^{k2}}{\sum_{rg}^{k2}\Delta x_k^4}\right)$$

$$a_{13}=a_{14}=a_{23}=a_{24}=c_{13}=c_{14}=c_{23}=c_{24}=\left(\frac{20D_g^k}{\sum_{rg}^k\Delta x_k\Delta y_k}+\frac{840D_g^{k2}}{\sum_{rg}^{k2}\Delta x_k^3\Delta y_k}\right)$$

$$a_{15}=a_{16}=a_{25}=a_{26}=c_{15}=c_{16}=c_{25}=c_{26}=\left(\frac{20D_g^k}{\sum_{rg}^k\Delta x_k\Delta z_k}+\frac{840D_g^{k2}}{\sum_{rg}^{k2}\Delta x_k^3\Delta z_k}\right)$$

$$a_{31}=a_{32}=a_{41}=a_{42}=c_{31}=c_{32}=c_{41}=c_{42}=\left(\frac{20D_g^k}{\sum_{rg}^k\Delta y_k\Delta x_k}+\frac{840D_g^{k2}}{\sum_{rg}^{k2}\Delta y_k^3\Delta x_k}\right)$$

$$a_{33}=a_{44}=\left(1+\frac{32D_g^k}{\Delta y_k}+\frac{120D_g^k}{\sum_{rg}^k\Delta y_k^2}+\frac{960D_g^{k2}}{\sum_{rg}^k\Delta y_k^3}+\frac{840D_g^{k2}}{\sum_{rg}^{k2}\Delta y_k^4}\right)$$

$$c_{33}=c_{44}=\left(1-\frac{32D_g^k}{\Delta y_k}+\frac{120D_g^k}{\sum_{rg}^k\Delta y_k^2}-\frac{960D_g^k}{\sum_{rg}^k\Delta y_k^3}+\frac{840D_g^{k2}}{\sum_{rg}^{k2}\Delta y_k^4}\right)$$

$$a_{34}=a_{43}=\left(\frac{8D_g^k}{\Delta y_k}+\frac{60D_g^k}{\sum_{rg}^k\Delta y_k^2}+\frac{720D_g^{k2}}{\sum_{rg}^k\Delta y_k^3}+\frac{840D_g^{k2}}{\sum_{rg}^{k2}\Delta y_k^4}\right)$$

$$c_{34}=c_{43}=\left(-\frac{8D_g^k}{\Delta y_k}+\frac{60D_g^k}{\nu_{rg}^k\Delta y_k^2}-\frac{720D_g^{k2}}{\sum_{rg}^k\Delta y_k^3}+\frac{840D_g^{k2}}{\sum_{rg}^{k2}\Delta y_k^4}\right)$$

$$a_{35}=a_{36}=a_{45}=a_{46}=c_{35}=c_{36}=c_{45}=c_{46}=\left(\frac{20D_g^k}{\sum_{rg}^k\Delta y_k\Delta z_k}+\frac{840D_g^{k2}}{\sum_{rg}^{k2}\Delta y_k^3\Delta z_k}\right)$$

$$a_{51}=a_{52}=a_{61}=a_{62}=c_{51}=c_{52}=c_{61}=c_{62}=\left(\frac{20D_g^k}{\sum_{rg}^k\Delta z_k\Delta x_k}+\frac{840D_g^{k2}}{\sum_{rg}^{k2}\Delta z_k^3\Delta x_k}\right)$$

$$a_{53}=a_{54}=a_{63}=a_{64}=c_{53}=c_{54}=c_{63}=c_{64}=\left(\frac{20D_g^k}{\sum_{rg}^k\Delta z_k\Delta y_k}+\frac{840D_g^{k2}}{\sum_{rg}^{k2}\Delta z_k^3\Delta y_k}\right)$$

$$a_{55}=a_{66}=\left(1+\frac{32D_g^k}{\Delta z_k}+\frac{120D_g^k}{\sum_{rg}^k\Delta z_k^2}+\frac{960D_g^{k2}}{\sum_{rg}^k\Delta z_k^3}+\frac{840D_g^{k2}}{\sum_{rg}^{k2}\Delta z_k^4}\right)$$

$$c_{55}=c_{66}=\left(1-\frac{32D_g^k}{\Delta z_k}+\frac{120D_g^k}{\sum_{rg}^k\Delta z_k^2}-\frac{960D_g^k}{\sum_{rg}^k\Delta z_k^3}+\frac{840D_g^{k2}}{\sum_{rg}^{k2}\Delta z_k^4}\right)$$

$$a_{56}=a_{65}=\left(\frac{8D_g^k}{\Delta z_k}+\frac{60D_g^k}{\sum_{rg}^k\Delta z_k^2}+\frac{720D_g^{k2}}{\sum_{rg}^k\Delta z_k^3}+\frac{840D_g^{k2}}{\sum_{rg}^{k2}\Delta z_k^4}\right)$$

$$c_{56}=c_{65}=\left(-\frac{8D_g^k}{\Delta z_k}+\frac{60D_g^k}{\sum_{rg}^k\Delta z_k^2}-\frac{720D_g^{k2}}{\sum_{rg}^k\Delta z_k^3}+\frac{840D_g^{k2}}{\sum_{rg}^{k2}\Delta z_k^4}\right)$$

$$b_{11}=b_{21}=\left(\frac{20D_g^k}{\sum_{rg}^k\Delta x_k}+\frac{840D_g^{k2}}{\sum_{rg}^{k2}\Delta x_k^3}\right)\quad b_{12}=-b_{22}=\frac{60D_g^k}{\sum_{rg}^k\Delta x_k}\quad b_{13}=b_{23}=\frac{140D_g^k}{\sum_{rg}^k\Delta x_k}$$

$$b_{31}=b_{41}=\left(\frac{20D_g^k}{\sum_{rg}^k\Delta y_k}+\frac{840D_g^{k2}}{\sum_{rg}^{k2}\Delta y_k^3}\right)\quad b_{34}=-b_{44}=\frac{60D_g^k}{\sum_{rg}^k\Delta y_k}\quad b_{35}=b_{45}=\frac{140D_g^k}{\sum_{rg}^k\Delta y_k}$$

$$b_{51}=b_{61}=\left(\frac{20D_g^k}{\sum_{rg}^k\Delta z_k}+\frac{840D_g^{k2}}{\sum_{rg}^{k2}\Delta z_k^3}\right)\quad b_{56}=-b_{66}=\frac{60D_g^k}{\sum_{rg}^k\Delta z_k}\quad b_{57}=b_{67}=\frac{140D_g^k}{\sum_{rg}^k\Delta z_k}$$

$$b_{14}=b_{15}=b_{16}=b_{17}=b_{24}=b_{25}=b_{26}=b_{27}=b_{32}=b_{33}=b_{36}=b_{37}=b_{42}=b_{43}=b_{46}=b_{47}=b_{52}=b_{53}=b_{54}=b_{55}=b_{62}=b_{63}=b_{64}=b_{65}=0$$

References

Argonne Code Center, June, 1977. Benchmark Problem Book, Report ANL-7416, Suppl. 2. Argonne National Laboratory, Argonne, IL.

Askew, J.R., Fayer, F.J., Kemshell, P.B., 1966. A general description of lattice code WIMSD. Journal of the British Nuclear Energy Society 5 (4), 564.
Delp, D.L., Harriman, J.M., Stedwell, M.J., 1964. FLARE-A Three-Dimensional Boiling Water Reactor Simulator (No. GEAP-4598). General Electric Co. Atomic Power Equipment Dept., San Jose, Calif.
National Energy Software Center, December, 1985. Benchmark Problem Book, Report ANL-7416, Suppl. 3. Argonne National Laboratory, Argonne, IL.
Finnemann, H., 1975. A Consistent nodal method for the analysis of space-time effects in large LWR's. In: Proc. Joint NEACRP/CSNI Specialist's Meeting on New Developments in Three-Dimensional Neutron Kinetics and Review of Kinetics Benchmark Calculations, MRR 145 (1975), Munich, January 22–24, pp. 131–172.
Finnemann, H., Bennewitz, F., Wagner, M.R., 1977. Interface current techniques for multidimensional reactor calculations. Atomkernenergie 30 (2), 123–128.
Goldstein, L., Nakache, F., Veras, A., 1967. Calculation of Fuel-Cycle Burnup and Power Distribution of Dresden-I Reactor with the TRILUX Fuel Management Program. United Nuclear Corp., Elmsford, NY.
Grundmann, U., Mittag, S., Kliem, S., 2005. DYN3D Version 3.2 – Code for Calculation of Transients in Light Water Reactors (LWR) with Hexagonal or Quadratic Fuel Elements-Description of Models and Methods, Report FZR-434, Forschungszentrum Rossendorf, Germany.
IAEA-TECDOC-233, 1980. Research Reactor Core Conversion from the Use of Highly Enriched Uranium to the Use of Low Enriched Uranium Fuels Guidebook.
IAEA-TECDOC-643, 1992. Research Reactor Core Conversion Guidebook, Volume 3: Analytical Verification (Appendices G and H).
Jagannathan, V., 1983. Evaluation of the finite-element-synthesis model using the 3-D finite-element technique. Annals of Nuclear Energy 10 (11), 569–578.
Lathrop, K.D., Brinkley, F.W., 1970. Theory and Use of the General Geometry TWOTRAN Program, Los Alamos Scientific Laboratory, LA-4432.
Lawrence, R.D., 1979. A Nodal Green's Function Method for Multidimensional Neutron Diffusion Calculations, Thesis, Nuclear Engineering Program, Univ. of Illinois, Urbana.
Lawrence, R.D., 1986. Progress in nodal methods for the solution of the neutron diffusion and transport equations. Progress in Nuclear Energy 17 (3), 271–301.
Menon, S.V.G., Khandekar, D.C., Trasi, M.S., 1981. Iterative Solutions of Finite Difference Diffusion Equations, BARC-1129.
Micheelson, B., Neltrup, H., 1973. The 3-D IAEA Benchmark Problem, Report RISO-M-1572.
Michels, H., 1997. DISLIN Manual. Max-Planck-Institut fur Aeronomie, Katlenburg-Lindau, 288. < http://www.dislin.de/> (last accessed 03.06.13).
Shober, R.A., Henry, A.F., 1976. Approximate analytical method for determining nodal fluxes. [BWR; PWR]. Transactions of the American Nuclear Society (United States), 24.
Shober, R.A., Sims, R.N., Henry, A.F., 1977. Two nodal methods for solving time-dependent group diffusion equations. Nuclear Science and Engineering (United States) 64 (2).
Sims, R.N., Henry, A.F., 1976. Coarse-mesh nodal method based on response matrix considerations [BWR; PWR]. Transactions of the American Nuclear Society (United States) 24.
Smith, K.S., 1986. Assembly homogenization techniques for light water reactor analysis. Progress in Nuclear Energy 17 (3), 303–335.
Zerkle, M.L., 1992. Development of a Polynomial Nodal Method with Flux and Current Discontinuity Factors, Phd Thesis. Massachusetts Institute of Technology.